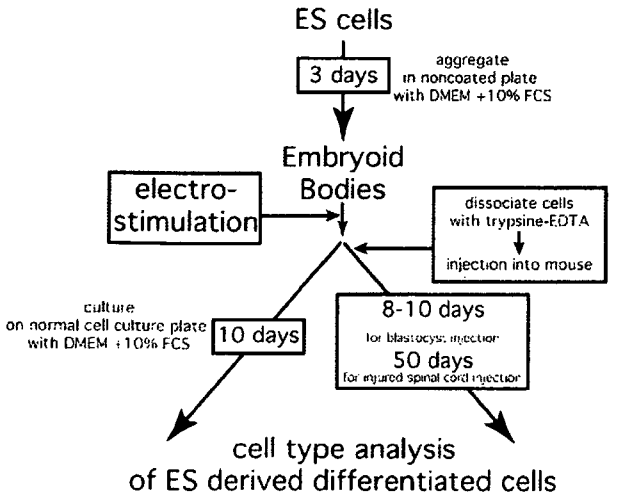

Figure 1. Experimental design. Embryoid bodies (EBs) were made by culturing embryonic stem (ES) cells with DMEM containing 10% FCS in noncoated bacterial petri dishes (Nunc). Electrical stimulation was applied to cells in a 4-mm gap cuvette under several voltage conditions (0, 5, 10, and 20 V; see supplemental data). For cell culture experiments, stimulated EBs were maintained in DMEM with 10% FCS on poly-D-Lysine-coated plates. For animal experiments, Venus-positive EBs were stimulated similarly (10 V, same 5-pulse train) and then dissociated with trypsin-EDTA for 3 minutes. Dissociated cells were injected into C57BL/6 blastocysts. Abbreviations: DMEM, Dulbecco's modified Eagle's medium; FCS, fetal calf serum.

http://www.invitrogen.com) on poly(D-lysine)-coated plates (BD, Franklin Lakes, NJ, http://www.bd.com). Ten days after stimulation, cells were fixed in paraformaldehyde in phosphate-buffered saline (pH 7.4) for immunocytochemical analyses. For animal experiments, Venus-positive EBs were stimulated similarly (10 V, same five-pulse train) and then dissociated with trypsin-EDTA for 3 minutes. Dissociated cells were injected into either mouse embryos or adult spinal cords.

Immunostaining

Cultured cells or histological sections were processed for immunostaining using the following antibodies: anti-TuJ1 mouse monoclonal antibody (mAb; 1:500; BAbCO, Berkeley, CA, http://www.babco.com), anti-GFP rat mAb (Nacalai, Kyoto, Japan, http://www.nacalai.co.jp), anti-Hu human polyclonal antibody (pAb; 1:1,000; a gift from Dr. Robert Darnell), anti-Ki67 rat mAb (DAKO, Glostrup, Denmark, http://www.dako.com), anti-MAP2 mouse mAb (1:200; Chemicon, Temecula, CA, http://www.chemicon.com), anti-ChAT rabbit pAb (1:200; Chemicon), anti-Islet1 mAb (1:400; Developmental Studies Hybridoma Bank [DSHB]), anti-Pax6 mAb (1:200; DSHB), anti-Pax7 mAb (1:400; DSHB), anti-MNR2 mAb (1:400; DSHB), and anti-Nkx2.2 mAb (1:400; DSHB). Histological sections were stained with the protocol described previously [16], and immunostained images were obtained with an LSM-510 confocal laser microscope (Carl Zeiss, Jena, Germany, http://www.zeiss.com/) by sequential scanning and analyzed with adjunctive software attached to the LSM-510. The thickness of the histological sections was less than 7 μm, and the z-axis sampling of the confocal images was less than 1 μm.

Measurement of Intracellular Ca^{2+} Concentration

ES cells or EBs were loaded with the Ca^{2+} fluorescence indicator fura-2 by incubating the cells in Hank's balanced salt solution (HBSS) containing 2 μM fura-2 AM (Molecular Probes Inc., Eugene, OR, http://probes.invitrogen.com) and 0.01% cremophor-EL (Sigma Chemicals, St. Louis, MO, http://www.sigmaaldrich.com/) at room temperature for 30 minutes. After loading, cells were washed in fresh HBSS and incubated an additional 15+ minutes before analysis of intracellular Ca^{2+} concentration ($[Ca^{2+}]_i$). $[Ca^{2+}]_i$ was analyzed with an inverted fluorescent microscope (IX-70, Olympus, Tokyo, http://www.olympus-global.com) equipped with a filter exchanger (Lambda 10-2, Sutter Instruments, Novato, CA, http://www.sutter.com/index.html) and a cooled charge-coupled device camera (MicroMax, Roper Scientific, http://www.roperscientific.com/). One train of five pulses (950-millisecond interpulse interval) was delivered with an electroporater (CUY459G20; Nepa Gene, Chiba, Japan, http://www.nepagene.jp). The following optics were used: excitation filter, 340HT15, and 380HT15; dichroic mirror, 430DCLP; emission filter, 510WT40 (all from Omega Optics, Austin, TX, http://www.omegaoptics.com/); and objective lens, Uapo/340 20x/0.75 (Olympus). Metafluor 5.0 software (Universal Imaging) was used to control the system and analyze acquired images [17].

Spinal Cord Injury Model

Spinal cord injury was induced with a modified NYU impactor as described previously [18]. Briefly, female C57BL/6J mice were anesthetized with an intraperitoneal injection of ketamine (100 mg/kg) and xylazine (10 mg/kg). After laminectomy at the T9 level, the dorsal surface of the dura matter was exposed. The vertebral column was stabilized with fine forceps and clamps at the T7 and T10 spinous processes and ligament, and then the animal's body was lifted. A 3-g weight (1.2-mm diameter tip) was allowed to drop from a height of 25 mm onto the dorsal surface of the dura matter. The muscles and the incision were then closed in layers, and the animals were placed in a temperature-controlled chamber until thermoregulation was reestablished. Manual bladder evacuation was performed twice per day until reflex bladder emptying was reestablished.

RESULTS

Cell Fate Determination of Electrically Stimulated Cells in Culture

We examined the influence of inter- and intracellular ionic balance on differentiation fate by application of weak electrical pulses. Embryoid bodies were stimulated at one of several intensities via an electrode (Fig. 1). The EBs were cultured for 10 days, and then fixed to assess differentiation fate (Fig. 1). Assessment for various markers (i.e., mainly for muscle and neural tissue) indicated that R1 ES cells showed no neuronal or myocytic differentiation, regardless of whether they were electrically stimulated (Fig. 2A, 2B, 2M, 2N). In contrast, EBs receiving electrical stimulation showed robust neuronal differentiation; control EBs (i.e., those receiving no stimulation) showed little differentiation (Fig. 2). Almost all colonies of EBs receiving 10-V stimulation contained cells immunoreactive for TuJ1, a marker for early committed neuronal cells, whereas less than 10% of control colonies contained TuJ1-positive cells derived from EBs receiving 0-V stimulation (Fig. 2A, 2C). We confirmed the neuronal identity of the cells from colonies that received 10-V stimulation: The majority of these cells were MAP2 immunoreactive (supplemental Fig. S1), whereas 20%–30% of cells showed immunoreactivity to MAP2 by retinoid treatment.

It is noteworthy that the neuronal cells in our system differentiated in a significantly shorter time than did those in most of other systems that use growth factors to initiate cell differentiation [5, 10, 11]. The differentiation efficiency decreased slightly in cells that received 20-V stimulation compared to that in cells that received milder stimulation. Although the morphology of these cells also clearly differed (e.g., thicker dendritic processes than in the ones receiving milder stimulation), all expressed TuJ1 (Fig. 2J). The size and number of colonies produced from cells stimulated with 20 V did not clearly differ from the size and number of colonies produced from the unstimulated cells. The size and number of colonies produced from

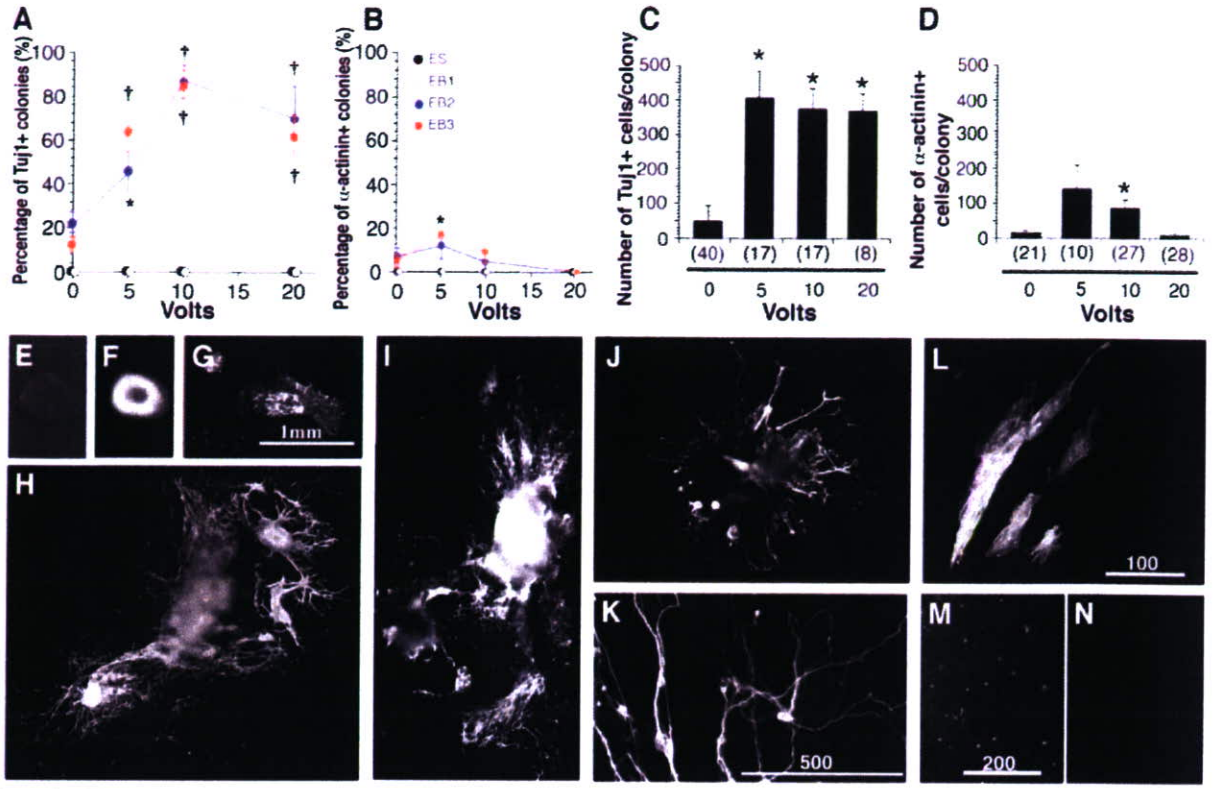

Figure 2. Effect of electrical stimulation on embryonic stem (ES) cell differentiation in culture. **(A–D):** Increasing, mild electrical stimulation disproportionately biases ES cell differentiation toward a neuronal fate. Percentage of colonies containing cells that express the neuronal marker TuJ1 **(A)**, and those that express the muscle marker α-actinin **(B)**: Black, filled circles, original ES cells; white open circles, ES cells cultured for 1 day to make embryoid bodies (EBs; before electrical stimulation); blue, filled circles, ES cells cultured for 2 days to make EBs (before electrical stimulation); and red, filled circles, ES cultured for 3 days to make EBs (before electrical stimulation). Number of TuJ1-positive cells per colony **(C)** and α-actinin-positive cells per colony **(D)**, both as a function of stimulation intensity. Daggers indicate $p < .001$ and asterisks indicate $p < .05$ compared to TuJ1-positive cells in zero-volt condition. Statistical differences between groups were assessed with Student's t test. A p value of at least $p < .05$ was considered significant. Numbers in parentheses in **(C)** and **(D)** indicate the number of colonies containing TuJ1-positive cells. **(E–G):** Appearance of unstimulated control EBs. Although the majority of colonies did not contain TuJ1-positive cells **(E)**, a few TuJ1-positive cells were present **(G)**. **(F):** Nuclear staining of EBs in **(E)** shows the density of cells. **(H–L):** Appearance of stimulated EBs. Anti-TuJ1 immunostaining of EBs subjected to either 5- **(H)**, 10- **(I)**, or 20-V **(J)** pulse stimulation. **(K):** Higher magnification of anti-TuJ1 immunostained EBs stimulated with 10 V. **(L):** Anti-α-actinin immunostained EBs stimulated with 10 V. **(M):** Nuclear staining demonstrates the existence of cells and lack of anti-TuJ1 immunostaining of ES cells. **(N):** Neuronal differentiation of ES cells was not induced. Nuclear stain was propidium iodide. Scale bars = 1 mm **(E–G)**, 100 μm **(H–J, L)**, 500 μm **(K)**, and 200 μm **(M, N)**.

cells stimulated with 5–15 V also did not differ. We note that the cell number and cell death did not show significant difference among EBs with or without electrical stimulation after outgrowth on the poly(D-lysine) plate (tunnel assay showed 11%–13% of cell death at 1 day and 3 days after outgrowth of EBs with electrical stimulation and without stimulation).

In general, we observed few muscle progenitors as a result of electrical stimulation, even though a slight but insignificant, increase in muscle progenitors was observed for EBs receiving 5-V stimulation (Fig. 2B, 2D). In addition, we did not observe cells differentiating into glial cells in our system (i.e., no glial fibrillary acidic protein [GFAP]-immunoreactive cells; supplemental Fig. S1). Electrical stimulation induced EBs to differentiate somewhat specifically into neuronal cells. However, because we failed to observe various differentiation markers (e.g., Islet1, Pax6, Pax7, MNR2, Nkx2.2, tyrosine hydroxylase, GAD65, Islet1) for specific neuronal cell types within 10 days of culture in immunocytochemical analysis, whereas we detected slight elevation of transcription of Pax6, NeuroD1, and some LIM-homeodomain genes by RT-PCR after 10 days of culture (data not shown), it is most likely that the TuJ1-positive cells of this ex vivo system did not reach the stage at which such neuronal markers are expressed.

Importance of Calcium Ion Influx for Modulation of Differentiation Fate

The mechanism that modulates fate determination in this system is unknown. To determine this mechanism, first, we examined the role of calcium by measuring intracellular Ca^{2+} concentration in ES cells and EBs before and after electrical stimulation (Fig. 3). It is well established that Ca^{2+} is an important signal transducer or modulator [19]. ES cells or EBs loaded with the fluorescent Ca^{2+} indicator fura-2 were electrically stimulated [17], and the resulting fluorescence was measured. ES cells showed no change in fluorescence emission after electrical stimulation, indicating that electrical stimulation did not induce release or uptake of Ca^{2+} in ES cells (Fig. 3B). In contrast, numerous cells within EBs showed small but significant changes in fluorescence after electrical stimulation, indicating that this stimulation induced an increase in Ca^{2+} concentration in EBs (Fig. 3A). Addition of the Ca^{2+} chelator EGTA (25 mM)

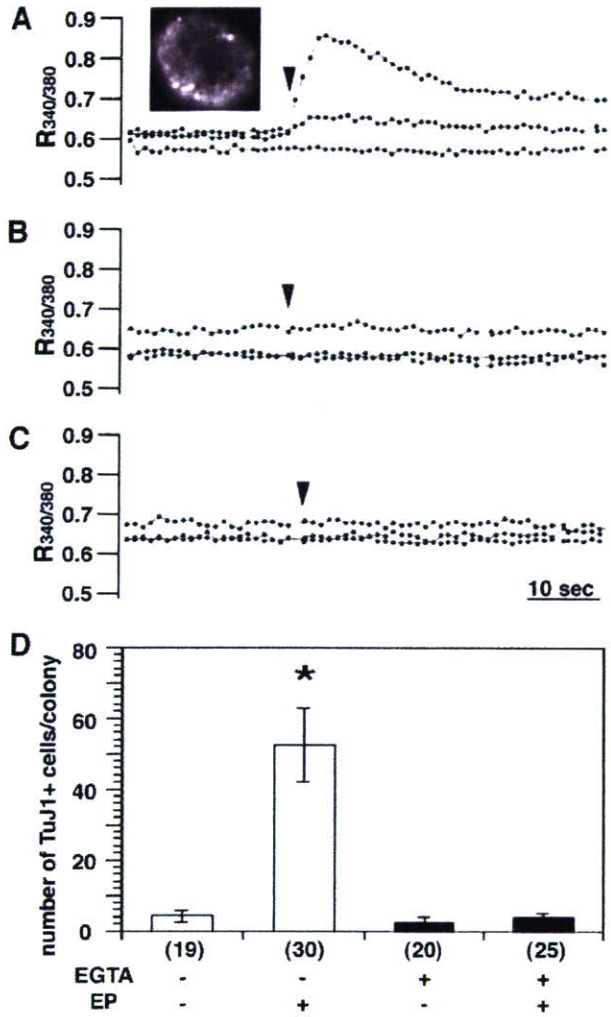

Figure 3. Electrical stimulation-induced calcium influx into cells. **(A–C):** Changes of $[Ca^{2-}]_i$ in embryoid bodies (EBs) **(A, B)** and in ES cells **(C)** after electrical stimulation. Ratio of fluorescence excitation intensities at 340 nm to 380 nm is plotted as a function of time. Filled arrowheads indicate time of electrical stimulation. Three typical patterns are displayed for each plot. Inset in **(A)** shows a fluorescent image of fura-2-loaded EBs excited at 380 nm. The culture medium contained either 2 mM Ca^{2+} **(A, C)** or 25 mM EGTA **(B)**. Cells were stimulated at 30 V (5–6 W) in this experiment. Due to the different buffer composition for this experiment, a higher voltage was required to produce comparable power (5–6 W) to that produced in the 10–15-V condition of the experiments presented in Figure 1. This stimulus intensity (one associated with 5–6 W) induces neuronal differentiation. **(D)**: Mean number of neuronal cells counted per colony in the presence and/or absence of the calcium chelator EGTA and stimulation with electric pulses (EP). The number of neuronal cells decreased dramatically when Ca^{2+} was absent from the medium. The same stimulation condition that yielded TuJ1-positive cells failed to yield neuronal cells when 25 mM EGTA was added to the medium. Open bars show data for incubation without EGTA and closed bars with EGTA. Number of colonies counted is indicated in parentheses. Again, due to the difference in culture conditions in this experiment, cell growth was largely disturbed in comparison with the conditions used in the experiments of Figure 1. The absolute number of cells after culturing was approximately one-tenth of the number of cells in the experiments presented in Figure 1. Statistical differences between groups were assessed with the Student's t test. Error bars are SEM. $p = .00057$ for comparison (*) between stimulated EBs with EGTA present and stimulated EBs with EGTA absent.

to the EB culture medium before electrical stimulation prevented any measurable change in fura-2 fluorescence (Fig. 3C), indicating that the source of Ca^{2+} was extracellular rather than intracellular.

To determine the significance of Ca^{2+} influx for electrically induced neuronal differentiation, EBs were electrically stimulated in the presence or absence of EGTA, and then these were cultured in the absence of EGTA and monitored for signs of differentiation fate. EBs electrically stimulated in the presence of EGTA failed to assume a neuronal fate, whereas those stimulated in the absence of EGTA assumed a neuronal fate (Fig. 3D). These results indicate that Ca^{2+} influx is, at the very least, necessary for neuronal cell fate determination in this system.

It is possible that this Ca^{2+} influx was not mediated by ionic channels, but instead, simply by physical disruption of the cell membranes caused by electrical stimulation. We believe that the latter is unlikely, because the emission ratio for fura-2 was significantly lower in electrically stimulated cells compared to that in cells with membrane fractures (Fig. 3A), suggesting that the increased Ca^{2+} influx did not result from passive influx caused by membrane fractures. In addition, we observed no blue staining in the cells when we applied trypan blue to the culture medium at the time of stimulation with parameters that successfully induced neuronal differentiation. However, we did observe staining in cells stimulated with higher voltage pulses (data not shown). The lack of trypan blue staining with milder stimulation parameters indicates that our parameters were sufficiently weak to avoid membrane fractures. Thus, the increased Ca^{2+} influx we observed was most likely mediated by Ca^{2+} ion channels, which probably play a key role in fate determination in our model system. However, we could not determine the type of Ca^{2+} channel at work in this system by applying inhibitors such as nifedepine or ω-conotoxin MVIIC. In addition, we could not detect significant expression of subunits from either of Ca^{2} channels L, N, and P/Q types, by reverse transcriptase polymerase chain reaction (RT-PCR) analysis on EB after 3 days of aggregation (data not shown).

Incorporation of Electrically Stimulated ES Cells into Neural Tissues of Embryos

To determine whether electrically stimulated EBs were capable of differentiating into mature neurons in vivo, stimulated or unstimulated EBs were injected into mouse embryos, and the fate of these cells was traced during the course of embryonic development. In this set of experiments, we used an ES cell line ubiquitously expressing Venus, an enhanced yellow fluorescent protein derivative [14]. When injected into mouse blastocysts, line LCVL10 ES cells incorporated equally into the bodies of embryos and neonatal mice. As before, ES cells expressing Venus were induced to make EBs, which were then either stimulated with 10-V pulses or were unstimulated, and then injected into mouse blastocysts (supplemental Fig. S2). Thirteen embryos and 15 embryos were recovered from the 10-V and unstimulated conditions, respectively.

Unstimulated EBs failed to incorporate into specific tissues in most embryos tested (10 of the 11-days-postcoitum [dpc] embryos and five of the 13-dpc embryos; supplemental Fig. S2). We observed fluorescence nonspecifically across the embryo and in extraembryonic structures, such as in the yolk sac of two embryos (one from 11-dpc and the other from 13-dpc embryos; supplemental Fig. S2; supplemental Table S2). The 11-dpc embryo that ES cells heavily contributed showed abnormality (supplemental Fig. S2). In two other 11-dpc embryos, strong fluorescence was observed only in the yolk sac, whereas virtually none was observed

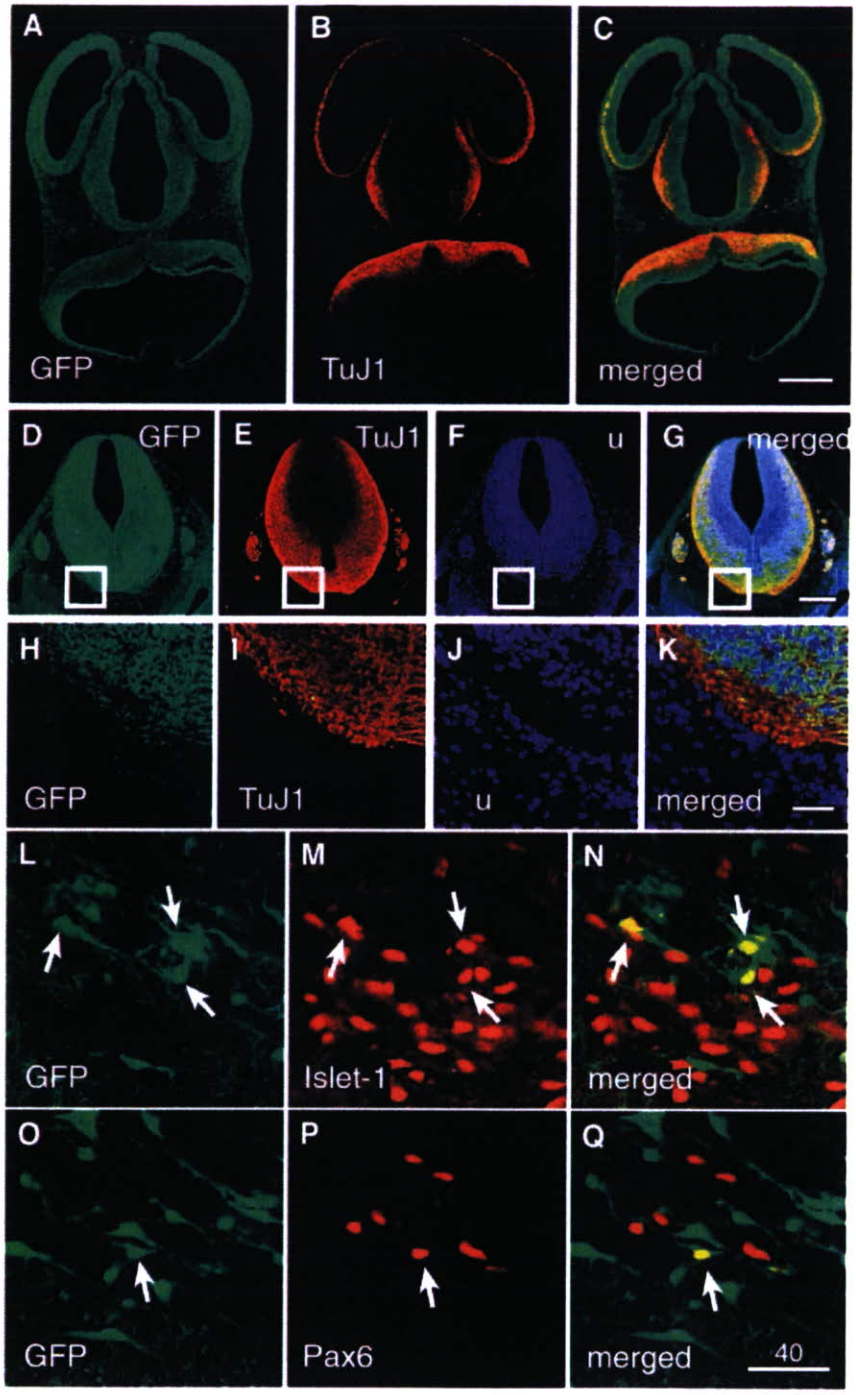

Figure 4. Distribution of electrically stimulated embryonic stem (ES) cells implanted in mouse embryos. An embryo at 11 days postcoitum (dpc) was sectioned to examine cell-type specificity of incorporated fluorescent ES cells in the central nervous system (CNS). Incorporation of ES cells into brain **(A–C)** and spinal cord **(D–Q)**, shown in transverse sections. Green fluorescent puncta are anti-GFP-positive cells expressing Venus **(A, C, D, G, H, K)**, red are TuJ1-positive cells, indicating differentiated neurons **(B, E, G, I, J)**, and blue shows nuclear staining with TO-PRO3 (Molecular Probes) **(F, G, J, K)**. Small boxes in **D–G** show areas of high magnification presented in **H–K**, respectively. **(L–Q)** High magnification images of a 13-dpc embryo showing that ES cells differentiated into a variety of neuron types, including motor neurons, interneurons, or their precursors. Green signals represent GFP, and red signals, Islet1 **(L–N)**, Pax6 **(O–Q)**. Scale bars = 500 μm **(A–C)**, 250 μm **(D–G)**, 50 μm **(H–K)**, and 40 μm **(L–Q)**. Abbreviation: GFP, green fluorescent protein.

in the embryo proper (data not shown). In the remaining 11 embryos, EBs did not incorporate (data not shown).

Cells arising from the stimulated EBs (EPs) tended to incorporate into neural tissue (supplemental Fig. S2; supplemental Table S2). We recovered nine embryos at 11 dpc and four embryos at 13 dpc. All of these recovered embryos were morphologically normal. Upon closer examination in whole-mount preparations, fluorescence appeared to be primarily localized to dorsal structures (i.e., the central nervous system [CNS]) in seven embryos (four of the 11-dpc embryos and three of the 13-dpc embryos) with small pockets of fluorescence in other structures, including the peripheral nervous system (PNS). In addition, in two of the 11-dpc embryos, we observed minor fluorescence in the PNS. For one embryo acquired at 13 dpc, the heart emitted strong fluorescence, and the PNS emitted weak fluorescence (supplemental Table S2). In summary, we observed that ES-derived Venus positive cells contributed primarily to CNS in 7 embryos among 13 recovered embryos when electrical stimulation is applied.

To determine whether incorporated EBs differentiated into proper neurons, we assessed several neuronal markers immunohistochemically. Transverse sections of two embryos recovered

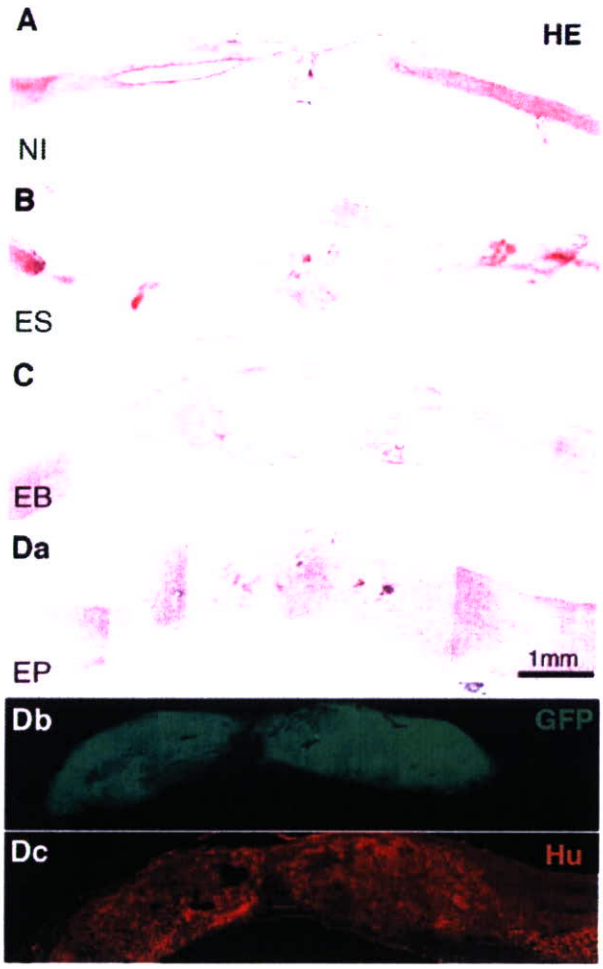

Figure 5. Longitudinal sections of injured, adult mouse spinal cords injected with electrically stimulated or nonstimulated cells. **(A–D):** Hematoxylin-eosin staining. Injured spinal cords 57 days after trauma was induced without injection of ES cells (ES; control) **(A)**. **(B–D):** Untreated or treated ES cells were injected 7 days after injury. Histological analysis was performed 50 days after injection with unstimulated ES cells **(B)**, with nonstimulated EBs **(C)**, or stimulated EBs (EP) **(D)**. Scale bar = 1 mm. **(D):** Incorporation of electrically stimulated EBs into injured adult spinal cord. **(Db):** Cells derived from stimulated EBs (EP) are positive for GFP. **(Dc):** ES cells from stimulated EBs differentiated into Hu-positive neuronal cells. Abbreviations: EB, embryoid body; EP, electropulsed; ES, embryonic stem; GFP, green fluorescent protein.

as 11 dpc and one from 13-dpc embryo were prepared and double immunostained for GFP and one of the following neuronal makers: TuJ1, Islet1, Pax6 (Fig. 4), LIM3, Pax7, or MNR2 [20]. All three preparations of CNS structures clearly contained numerous double-immunostained cells, as shown in Figure 4, for Islet1 and Pax6 (i.e., cells that were immunoreactive for both GFP and one of the above-mentioned neuronal markers), suggesting that, in vivo, cells from electrically stimulated EBs can differentiate into proper functional neurons. Although electrically stimulated cells tended to incorporate into ventral spinal cord to form motor neurons and interneurons, they can, in principle, incorporate into various neural structures across the dorsoventral axis to form different types of mature neurons (Fig. 4). With respect to the anteroposterior axis, we also found GFP-labeled cells in forebrain, hindbrain, brain stem, and spinal cord (Fig. 4).

Together, our data demonstrate that electrically stimulated EBs differentiate primarily into early committed neuronal cells. These cells are plastic and can differentiate into a variety of specific neuronal cell types in accordance with the environment.

Electrically Stimulated EBs Contribute to Injured Adult Spinal Cords

Our embryo experiments prompted us to examine whether electrically stimulated EBs are capable of differentiating into neurons when grafted into the injured spinal cords of adult mice. Stimulated EBs produced from Venus-expressing ES cells were injected into spinal cords of mice 7 days after injury, and their survival and phenotype within the spinal cord was assessed 50 days after transplantation (Fig. 5D). As control experiments, we also grafted unstimulated EBs or unstimulated ES cells into the spinal cords of adult mice (Fig. 5A–5C). In each animal, 10^6 cells were injected in a volume of 5 μl. Of the five animals injected with stimulated EBs, one failed to survive due to injury, and all of the others showed evidence of incorporation into the spinal cord as neuronal cells. Two of five animals injected with unstimulated EBs and three of six animals injected with unstimulated ES cells died within 50 days. All of the survivors from both of these control experiments showed tumorigenic or pathogenic features (Fig. 5B, 5C).

Immunostaining revealed that a large part of electrically stimulated EBs were capable of differentiating into Hu-positive neuronal cell types (Fig. 5D; Fig. 6A–6D). We detected no cells that differentiated into GFAP-positive astrocytes or NG2-positive oligodendrocytes (data not shown). In these experiments, approximately 80% of grafted cells assumed a neuronal lineage, clearly expressing neural markers including Hu (Fig. 6A–6D, 6M). Furthermore, Venus-positive cells also immunostained for MAP2, indicating that the exogenous cell population differentiated into neurons (Fig. 7A–7C). On the contrary, even surviving animals possessed few Hu-positive neuron-like cells derived from unstimulated EBs or ES cells (Fig. 6E–6M). Notably, in all the survivors, we observed pathology within the grafts (e.g., infiltration of inflammatory cells, such as macrophages, or ectopically formed tubular structures surrounded by epithelia-like cells; Fig. 5B, 5C). In both cases, many of the injected cells were reactive for phosphorylated histone H3 (phospho-H3) or Ki67 antibodies, suggesting that the grafted cells maintained proliferative activity and thus can be tumorigenic (Fig. 6E–6L, 6N). On the other hand, stimulated EBs showed essentially no phospho-H3 and Ki67 immunoreactivity (Fig. 6A–6D, 6N).

In summary, stimulated EBs contributed robustly to form neurons within the spinal cord, whereas unstimulated and stimulated ES cells, as well as unstimulated EBs, formed few neurons (Fig. 5). In addition, grafts appeared to display pathological features (Fig. 5).

To analyze in more detail the fate of these neural cells, we performed additional immunohistochemical analyses using antibodies against several neuronal markers. ChAT and Islet1, markers found in spinal motor neurons, colocalized within Venus-expressing cells (Fig. 7D–7F; data not shown) [21], indicating that grafted cells have the potential to differentiate into motor neurons. We detected a few parvalbumin- and γ-aminobutyric acid-positive cells among the Venus-expressing cells that displayed typical neuron-like morphology (Fig. 7G–7I; data not shown). Stimulated EBs incorporated quite well into spinal cord tissues, differentiating into a variety of neuronal cell types and mixing with the recipients' own cells (Fig. 7).

These experiments with injured spinal cord established that stimulated EBs are capable of differentiating into mature neu-

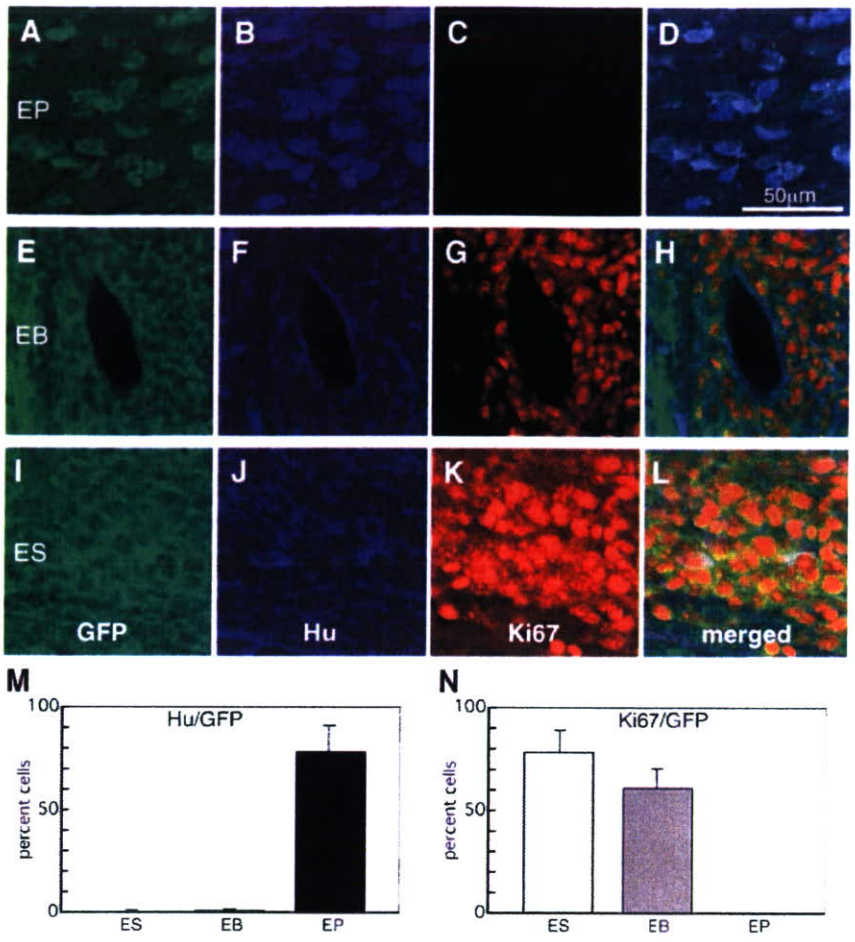

Figure 6. Stimulated EBs frequently adopted the appearance of neuronal cells when injected into spinal cord. **(A–D):** Almost all the cells derived from stimulated EBs (EP) displayed Hu immunoreactivity but not Ki67 immunoreactivity, whereas cells derived from unstimulated EBs (EB; **E–H**) or ES cells **(I–L)** displayed Ki67 immunoreactivity but not Hu immunoreactivity. **(M):** Graph showing the percentage of cells that coexpress both GFP and Hu. **(N):** Graph showing the percentage of cells that coexpress both GFP and Ki67. Percentages indicated were average of percentages of Hu- or Ki67-positive cell counts obtained by tallying the GFP-positive cells observed in more than 10 different focal planes of each EP, EB, and ES examined. Green, blue, and red signals indicate GFP, Hu, and Ki67 immunoreactivity, respectively **(A–L)**. Scale bar = 50 μm. Abbreviations: EB, embryoid body; EP, electropulsed; ES, embryonic stem; GFP, green fluorescent protein.

rons when inserted into an in vivo environment. It is possible that injury to the spinal cord provided environmental cues necessary to direct differentiation. This hypothesis is supported by findings that adult neuronal stem cells differentiate into glial cells in response to spinal cord injury [22–24]. Growth factors and cytokines are released, and these factors, in turn, can modulate proliferation and differentiation of neuronal stem cells [25–28].

DISCUSSION

ES cells that have initiated differentiation steps will preferentially assume a neuronal fate when electrically stimulated. In comparison with other systems that produce neural cells from ES cells, the neuronal cells in our system differentiated in a significantly shorter period than did those produced by other methods [5, 10, 11]. Moreover, these stimulated ES cells could be easily transplanted into animal tissues. According to our observations, the differentiation process can be divided into three steps: (a) destabilization of undifferentiated ES cells, (b) modulation of cell fate direction, and (c) differentiation to a mature, terminal cell state. Unlike other induction methods, electrical stimulation seems to work only during the second step. There are several reports on electrical stimulation-induced neurite extension and growth cone guidance cue of PC12 cells or some neural cells [29–33], which are mostly destined to neural fate, but not pluripotent, as ES cells are. In these reports, electrical stimulation alters their morphology, which probably corresponds to the third or even later phase of developmental process in this scheme.

These cells possess terminal differentiation plasticity, requiring further steps to determine a neuronal destiny. They failed to express any specific markers indicative of mature neurons ex vivo, and were flexible or plastic; thus, the differentiation course of these multipotent cells can be further molded by the environmental context and can differentiate into cells suitable for the region in which they have been transplanted. Indeed, the cells derived from treated EBs showed varied neural specificities, both when injected into blastocysts and when implanted into adult spinal cords. Electrically stimulated EBs seem to incorporate into the CNS with no specific preference for anterior-posterior or dorsoventral axes, as we observed that the injected cells contributed to the entire CNS in our blastocyst injection experiments. Some induction protocols may specifically direct cells to preferentially contribute to certain tissues. For example, the protocol that uses retinoids directs cells to differentiate toward cell types located in posterior structures [34].

A large proportion of the cells (approximately 80%) derived from stimulated EBs displayed neuronal identities when injected into injured spinal cord, an environment that is non-neurogenic (Fig. 5). This amount of neural differentiation is extremely high in comparison with that observed by Ogawa et al. [35], who adopted a similar experimental design with in vitro expanded neural stem/progenitor cells derived from fetal spinal cord. In the present study, the cells we grafted differentiated into various types of neurons, as

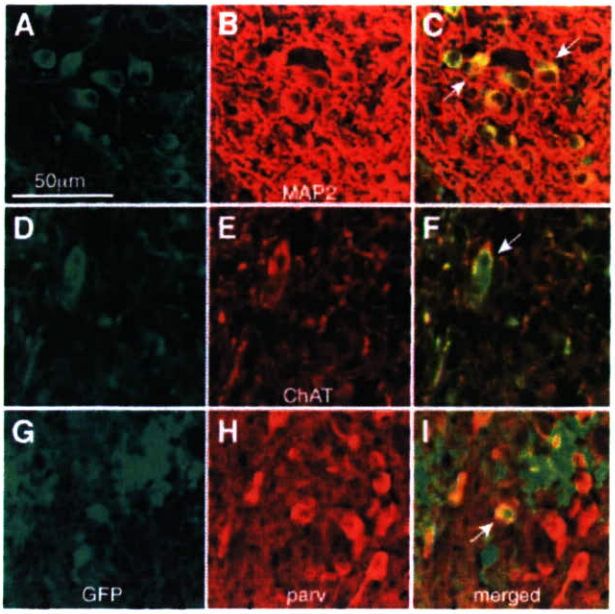

Figure 7. Stimulated embryoid bodies (EBs) adopted the appearance of various types of neuronal cells when injected into spinal cord. **(A–C):** Almost all the cells derived from stimulated EBs (electropulsed [EP]) displayed MAP2 immunoreactivity, indicating that they had differentiated into mature neurons. Some of the cells derived from EPs expressed ChAT, a motor neuron marker **(D–F)**, or parvalbumin, an inhibitory neuron marker **(G–I)**. Scale bar = 50 μm.

indicated by expression of several markers including neurotransmitters. Importantly, stimulated EBs showed almost no proliferative activity 50 days after transplantation, unlike ES cells or unstimulated EBs, which showed proliferative and pathogenic features (Fig. 6). Because cells derived from stimulated EBs were extremely efficient in assuming a course of neuronal differentiation in an in vivo environment, they hold much promise for use in therapeutic applications.

Ca^{2+} is one of the most important signaling ions involved in various biological activities [19]. Ca^{2+} also appears to play an important role in the system we studied. We found that Ca^{2+} influx was necessary for neural fate determination of EBs. Our finding indicates that this influx did not result from cell membrane fissures; rather, it appears that Ca^{2+} channels may be responsible for Ca^{2+} uptake in our system for the three following reasons: (a) passive influx via membrane fractures results in a much higher magnitude of intracellular fluorescence than what we observed in this study, (b) dye in the culture medium failed to enter the cells upon electrical stimulation, and (c) the original ES cells that did not take on a neuronal fate after electrical stimulation showed no evidence of Ca^{2+} influx (Fig. 3C). We attempted to identify these Ca^{2+} channels by culturing electrically stimulated EBs in media containing agents that block three major Ca^{2+} channels. Treatment with nifedepine, an L-type Ca^{2+} channel blocker, and ω-conotoxins, N- and P/Q-type blockers, failed to block Ca^{2+} influx. Although the existence of these major Ca^{2+} channels in EBs could not be excluded, we conclude that EBs most likely express other minor Ca^{2+} transporters and that these channels mediate the Ca^{2+} influx necessary for neuronal cell fate determination in this system. We conclude that EB formation is required for activation of these Ca^{2+} ion transporters, because, unlike EBs, ES cells showed no change in intracellular Ca^{2+} density after electrical stimulation.

Ca^{2+} is also known to be involved in the noncanonical *Wnt* signaling pathway. In *Xenopus* and zebrafish, some Wnt ligands stimulate release of intracellular Ca^{2+} during development [36]. This Ca^{2+} release, however, induces differentiation into elements (e.g., non-neuronal cells) fated to become ventrally located structures [37]. This is in stark contrast to our system, in which Ca^{2+} induces differentiation into elements (e.g., neuronal cells) fated to become dorsally located structures.

In spite of our efforts, we do not fully understand the mechanisms for this differentiation system. Although we successfully demonstrated that the Ca^{2+} flux is required for the induction (Fig. 3), this will not fully interpret the system. It is possible that other ions, such as potassium or sodium, can also be involved [38]. We are underway to further understand the mechanisms of neuronal induction ability of electrical stimulation on ES cells.

Signaling pathways that transmit information out of cells into the environment are usually activated by receptor-ligand recognition. However, in the present experiments, physical alteration of cell surface membranes may initiate signaling, even though the normal signaling molecule takes over later. This primitive signaling pathway may be a prototype that mediates environmental effects on cells. Receptor-ligand signaling systems may have evolved for stabilization and refinement of environmental cues impinging on cells. This simple system may possibly be invoked during early development and neuronal regeneration. In neuronal tissues, ionic currents are continuously flowing, and these currents may instruct and ensure that undifferentiated cells assume the fate of neuronal progenitors. Ionic flux, therefore, may be a novel category of differentiation signals. Indeed, recent findings show that excitatory neural activity induces adult neural stem cells to adopt a neural fate [39, 40]. In our study, we observed that cells affected by ionic currents were very close to being in an undifferentiated state. The effective differentiation step, therefore, corresponds to states that occur earlier than the neural stem cell state, because unstimulated cells could adopt various cell fates. Even though further studies are required to investigate the physiological role of ionic flow in early embryos, our observations suggest that transmembrane ion flow may play an integral role in early stages of development.

In summary, we described a simple and novel procedure for producing neural cells from ES cells. Further studies are needed to improve our procedure so that parameters are appropriate for therapeutic applications.

ACKNOWLEDGMENTS

We thank A. Nagy, J. Miyazaki, and R. Darnell for the gift of reagents. We also thank S. Itohara for sharing the ES cell facility, and N. Nakatani for useful discussions. Monoclonal antibodies against Islet1, Pax6, Pax7, MNR2, Nkx2.2, and Lim3 developed by T.M. Jessell were obtained from the Developmental Studies Hybridoma Bank under the auspices of NICHD and maintained by University of Iowa. T.K. thanks M. Muramatsu for continuous encouragement, I. Naganuma for secretarial work, and the late G. Matsumoto for help in establishing the laboratory. M.Y. is a recipient of a grant-in-aid for Young Scientists from The Ministry of Education, Culture, Sports, and Technology (MEXT) of Japan. T.K. is supported by a grant from the Human Frontier Scientific Program Orga-

nization and a grant-in-aid for Scientific Research on Priority Areas from MEXT of Japan. All mice were maintained at the animal facilities of RIKEN-BSI according to the Institution's guidelines.

REFERENCES

1 Miller-Hance WC, LaCorbiere M, Fuller SJ et al. In vitro chamber specification during embryonic stem cell cardiogenesis. J Biol Chem 1993;268:25244–25252.
2 Coucouvanis E, Martin GR. BMP signaling plays a role in visceral endoderm differentiation and cavitation in the early mouse embryo. Development 1999;126:535–546.
3 Gratsch TE, O'Shea KS. Noggin and Chordin have distinct activities in promoting lineage commitment of mouse embryonic stem cells. Dev Biol 2002;245:83–94.
4 Brustle O, Jones KN, Learish RD et al. Embryonic stem cell-derived glial precursors: A source of myelinating transplants. Science 1999;285: 754–756.
5 Lee SH, Lumelsky N, Studer L et al. Efficient generation of mid brain and hindbrain neurons from mouse embryonic stem cells. Nat Biotechnol 2000;18:675–679.
6 Lumelsky N, Blondel O, Laeng P et al. Differentiation of embryonic stem cells to insulin-secreting structures similar to pancreatic islets. Science 2001;292:1389–1394.
7 Zhang S-C, Wering M, Duncan ID et al. In vitro differentitation of transplantatable neuronal precursors from human embryonic stem cells. Nat Biotech 2001;19:1129–1133.
8 Kawasaki H, Mizuseki K, Nishikawa S et al. Induction of midbrain dopaminergic neurons from ES cells by stromal cell-derived inducing activity. Neuron 2000;28:31–40.
9 Tropepe V, Hitoshi S, Sirard C et al. Direct neural fate specification from embryonic stem cells: A primitive mammalian neural stem cell stage acquired through a default mechanism. Neuron 2001;30:65–78.
10 Wichterle H, Lieberam I, Porter JA et al. Directed differentiation of embryonic stem cells into motor neurons. Cell 2002;110:385–397.
11 Ying Q-L, Stavridis M, Griffiths D et al. Conversion of embryonic stem cells into neuroectodermal precursors in adherent monoculture. Nat Biotechnol 2003;21:183–186.
12 West AE, Chen WG, Dalva MB et al. Calcium regulation of neuronal gene expression. Proc Natl Acad Sci U S A 2001;98:11024–11031.
13 Zhang LI, Poo MM. Electric activity and development of neuronal circuits. Nat Neurosci 2001;4 Suppl:1207–1214.
14 Nagai T, Ibata K, Park ES et al. A variant of yellow fluorescent protein with fast and efficient maturation for cell-biological applications. Nat Biotechnol 2002;20:87–90.
15 Niwa H, Yamamura K, Miyazaki J. Efficient selection for high-expression transfectants with a novel eukaryotic vector. Gene 1991;108:193–199.
16 Tanemura K, Ogura A, Cheong C et al. Dynamic rearrangement of telomeres during spermatogenesis in mice. Dev Biol 2005;281:196–207.
17 Sawano A, Hama H, Saito N et al. Multicolor imaging of Ca(2+) and protein kinase C signals using novel epifluorescence microscopy. Biophys J 2002;82:1076–1085.
18 Okada S, Nakamura M, Mikami Y et al. Blockade of interleukin-6 receptor suppresses reactive astrogliosis and ameliorates functional recovery inexperimental spinal cord injury. J Neurosci Res 2004;76:265–276.
19 Crabtree GR, Olson EN. NFAT signaling: Choreographing the social lives of cells. Cell 2002;109:S67–S79.

DISCLOSURES

The authors indicate no potential conflicts of interest.

20 Tanabe Y, William C, Jessell TM. Specification of motor neuron identity by MNR2 homeodomain protein. Cell 1998;95:67–80.
21 Tsuchida T, Ensini M, Morton SB et al. Topographic organization of embryonic motor neurons defined by expression of LIM homeobox genes. Cell 1994;79:957–970.
22 Beattie MS, Bresnahan JC, Komon J et al. Endogenous repair after spinal cord contusion injuries in the rat. Exp Neurol 1997;148:453–463.
23 Johansson CB, Momma S, Clarke DL et al. Identification of a neural stem cell in the adult mammalian central nervous system. Cell 1999;96: 25–34.
24 Johansson CB, Lothian C, Molin M et al. Nestin enhancer requirements for expression in normal and injured adult CNS. J Neurosci Res 2002; 69:784–794.
25 Nakamura M, Bregman BS. Difference in neurotrophic factor gene expression profiles between neonate and adult rat spinal cord after injury. Exp Neurol 2001;169:407–415.
26 Okano H. The stem cell biology of the central nervous system. J Neurosci Res 2002;69:698–707.
27 Nakamura M, Houghtling RA, MacArthur L et al. Differences in cytokine expression profile between acute and secondary injury in adult rat spinal cord. Exp Neurol 2003;184:313–325.
28 Okano H, Ogawa Y, Nakamura M et al. Transplantation of neural stem cells into the spinal cord after injury. Semin Cell Dev Biol 2003;379:1–8.
29 Cohan CS. Frequency-dependent and cell-specific effects of electrical activity on growth cone movements of cultured Helisoma neurons. J Neurobiol 1990;21:400–413.
30 Nakae H. Morphological differentiation of rat pheochromocytoma cells (PC12 cells) by electric stimulation. Brain Res 1991;558:348–352.
31 Manivannan S, Terakawa S. Rapid sprouting of filopodia in nerve terminals of chromaffin cells, PC12 cells, and dorsal root neurons induced by electrical stimulation. J Neurosci 1994;14:5917–5928.
32 Aniksztejn L, Demarque M, Morozov Y et al. Recurrent CA1 collateral axons in developing rat hippocampus. Brain Res 2001;913:195–200.
33 McCaig CD, Rajnicel AM, Song B et al. Has electrical growth cone guidance found its potential? Trends Neurosci 2002;25:354–359.
34 Kessel M, Gruss P. Homeotic transformations of murine vertebrae and concomitant alteration of *Hox* codes induced by retinoic acid. Cell 1991;67:89–104.
35 Ogawa Y, Sawamoto K, Miyata T et al. Transplantation of in vitro expanded fetal neural progenitor cells results in neurogenesis and functional recovery after spinal cord contusion injury in adult rats. J Neurosci Res 2002;69:925–933.
36 Pandur P, Maurus D, Kuhl M. Increasingly complex: New players enter the Wnt signaling network. BioEssays 2002;24:881–884.
37 Kuhl M, Sheldahl LC, Malbon CC et al. Ca^{2+}/Calmodulin-dependent protein kinase II is stimulated by Wnt and Frizzled homologs and promotes ventral cell fates in *Xenopus*. J Biol Chem 2000;275:12701–12711.
38 Yamada M, Nakanishi K, Ohba S et al. Brain-derived neurotrophic factor promotes the maturation of GABAergic mechanisns in cultures hippocampal neurons. J Neurosci 2002;22:7580–7585.
39 Deisseroth K, Singla S, Toda H et al. Excitation-neurogenesis coupling in adult neural stem/progenitor cells. Neuron 2004;42:535–552.
40 Spitzer NC, Root CM, Borodinsky LN. Orchestrating neuronal differentiation: Patterns of Ca^{2+} spikes specify transmitter choice. Trends Neurosc 2004;27:415–421.

See www.StemCells.com for supplemental material available online.

THE JOURNAL OF BIOLOGICAL CHEMISTRY VOL. 281, NO. 8, pp. 5037–5041, February 24, 2006

Formation of Tau Inclusions in Knock-in Mice with Familial Alzheimer Disease (FAD) Mutation of Presenilin 1 (PS1)*

Received for publication, August 19, 2005, and in revised form, December 21, 2005 Published, JBC Papers in Press, December 23, 2005, DOI 10.1074/jbc.M509145200

Kentaro Tanemura[‡], Du-Hua Chui[‡1], Tetsuya Fukuda[‡], Miyuki Murayama[‡], Jung-Mi Park[‡], Takumi Akagi[§], Yoshitaka Tatebayashi[‡], Tomohiro Miyasaka[‡], Tetsuya Kimura[‡], Tsutomu Hashikawa[§], Yuka Nakano[¶], Takashi Kudo[¶], Masatoshi Takeda[¶], and Akihiko Takashima[‡2]

From the [‡]Laboratory for Alzheimer Disease and [§]Neural Architecture, Brain Science Institute, RIKEN, Wako, Saitama 351-0198, Japan and the [¶]Department of Psychiatry and Behavioral Science and Environmental Medicine, Osaka University Graduate School of Medicine, 2-2 Yamadaoka, Suita, Osaka 565-0871, Japan

Mutations in the presenilin 1 (*PS1*) gene are responsible for the early onset of familial Alzheimer disease (FAD). Accumulating evidence shows that PS1 is involved in γ-secretase activity and that FAD-associated mutations of PS1 commonly accelerate $A\beta_{1-42}$ production, which causes Alzheimer disease (AD). Recent studies suggest, however, that PS1 is involved not only in Aβ production but also in other processes that lead to neurodegeneration. To better understand the causes of neurodegeneration linked to the PS1 mutation, we analyzed the development of tau pathology, another key feature of AD, in PS1 knock-in mice. Hippocampal samples taken from FAD mutant (I213T) PS1 knock-in mice contained hyperphosphorylated tau that reacted with various phosphodependent tau antibodies and with Alz50, which recognizes the conformational change of PHF tau. Some neurons exhibited Congo red birefringence and Thioflavin T reactivity, both of which are histological criteria for neurofibrillary tangles (NFTs). Biochemical analysis of the samples revealed SDS-insoluble tau, which under electron microscopy examination, resembled tau fibrils. These results indicate that our mutant PS1 knock-in mice exhibited NFT-like tau pathology in the absence of Aβ deposition, suggesting that PS1 mutations contribute to the onset of AD not only by enhancing $A\beta_{1-42}$ production but by also accelerating the formation and accumulation of filamentous tau.

Alzheimer disease (AD)[3] is characterized pathologically by neurofibrillary tangles (NFTs), which are composed of highly phosphorylated tau, and by neuronal loss and Aβ deposition. AD is manifested symptomatically by dementia. Presenilin 1 (*PS1*), a gene identified to be responsible, in part, for early onset familial Alzheimer disease (FAD), has been cloned (1, 2). To date more than 70 mutations of the *PS1* gene have been reported (3, 4). In each mutation, early onset of AD develops with 100% penetration (3, 4). PS1 is required for γ-secretase to cleave amyloid precursor protein into Aβ species such as $A\beta_{1-40}$ and $A\beta_{1-42}$. Improper cleavage of amyloid precursor protein because of a PS1 mutation increases the production of $A\beta_{1-42}$ (5–7), a highly aggregative, neurotoxic species of Aβ that is longer than the less toxic $A\beta_{1-40}$. One hypothesis for the neurodegeneration observed in AD, therefore, is that PS1 mutation leads to increasing amounts of extracellular, neurotoxic $A\beta_{1-42}$, thereby inducing neurodegeneration (8–11).

Accumulating data suggest that, in addition to its role in $A\beta_{1-42}$ production, PS1 mutation also contributes to NFT formation. For example, PS1 conditional knock-out mice display phosphorylated tau, synaptic dysfunction, and memory impairment, even in the absence of Aβ production and deposition (12). In a related line of research, some patients clinically diagnosed with fronto-temporal dementia (FTD) have been shown to harbor PS1 mutations (13–16). Interestingly, FTD is characterized by the appearance of NFTs without Aβ deposition (17). A patient harboring the G183V PS1 mutation displayed the clinical manifestations of FTD and exhibited phospho-tau-positive Pick body pathology throughout the cortex and limbic region, without Aβ deposition. Other reports have also shown that PS1 mutations accelerate NFT formation and neuronal loss without affecting the rate of Aβ deposition (18). Thus, these data lead to the hypothesis that PS1 mutations might contribute to NFT formation as well as increase $A\beta_{1-42}$ production in FAD.

To investigate this hypothesis, we examined tau pathology in mutant PS1 I213T knock-in mice (19). This line of mice was generated with a targeted insertion of the I213T missense mutation into exon 7 of the mouse *PS1* gene using homologous recombination. Therefore, these PS1 mutant knock-in mice harbor the FAD mutation in the mouse *PS1* gene and produce PS1 I213T. Heterozygote mutant PS1 I213T mice showed no change in $A\beta_{1-40}$ levels but had increased levels of $A\beta_{1-42}$, a 1.3-fold increase when compared with wild-type mice. This $A\beta_{1-42}$ increase is comparable to that observed in human cases. Because this mouse strain shares the same PS1 genotype and related pathology as that of patients harboring the PS1 mutation, we initially expected these mice to develop the AD phenotype. The increase in murine $A\beta_{1-42}$, however, failed to lead to a corresponding Aβ deposition, possibly because murine Aβ has a different amino acid sequence that reduces its tendency to aggregate. Using this dissociation to our advantage, we investigated the Aβ deposition-independent effects of the PS1 mutation in this mouse model. We found that GSK-3β activation was followed by the accumulation of hyperphosphorylated tau in the hippocampal region, which fulfills the histological criteria for the presence of NFTs.

EXPERIMENTAL PROCEDURES

Animals—Mutant PS1 I213T knock-in mice (mPS1 mice) were maintained at the RIKEN BSI animal facilities according to the Institute guidelines for the treatment of experimental animals.

* This work was supported in part by a grant from the Ministry of Education, Science, Sports, and Culture of Japan. The costs of publication of this article were defrayed in part by the payment of page charges. This article must therefore be hereby marked "*advertisement*" in accordance with 18 U.S.C. Section 1734 solely to indicate this fact.

[1] Present address: Neuroscience Research Institute, Peking University, 38 Xue Yuan Rd., Beijing 100083, China.

[2] To whom correspondence should be addressed: Laboratory for Alzheimer Disease, RIKEN Brain Science Institute, 2-1 Hirosawa, Wako-shi, Saitama 351-0198, Japan. Tel.: 81-48-467-9632; Fax: 81-48-467-5916; E-mail: kenneth@brain.riken.jp.

[3] The abbreviations used are: AD, Alzheimer disease; PS1, presenilin 1; FAD, familial Alzheimer disease; Aβ, amyloid β protein; NFT, neurofibrillary tangles; FTD, fronto-temporal dementia; GSK-3β, glycogen synthase kinase-3β; PHFs, paired helical filaments; TBS, Tris-buffered saline; CDK5, cyclin-dependent kinase 5; JNK, c-Jun N-terminal kinase; MAP, mitogen-activated protein; TUNEL, terminal deoxynucleotidyltransferase-mediated dUTP nick end-labeling; RIPA, radioimmune precipitation assay buffer.

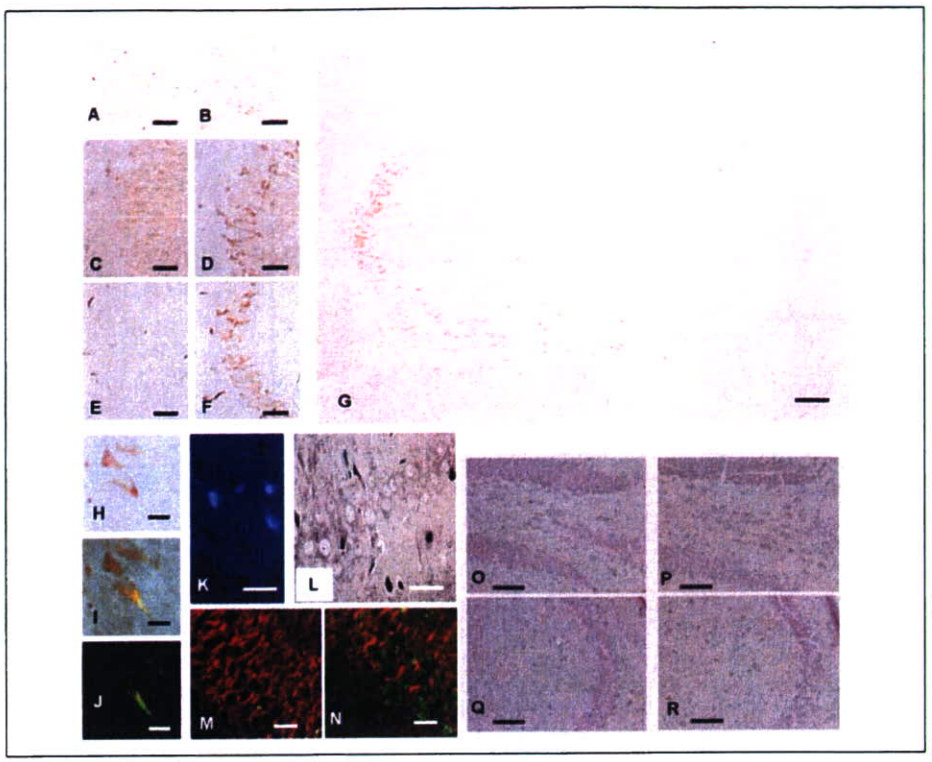

FIGURE 1. **Histochemical and histopathological assessment of brain sections from wild-type (wPS1) and mutant PS1 knock-in (mPS1) mice.** *A–G*, anti-tau immunoreactivity in hippocampal CA3 of wPS1 mice (*A, C, E*) and heterozygous mPS1 mice (*B, D, F*) at 7 months (*A, B*) and 15 months (*C–G*) of age. *A–D*, PS199 immunoreactivity; *E–G*, Alz50 immunoreactivity. The low power micrograph in *G* shows how hippocampal immunoreactivity is confined largely to CA3. *H–L*, histopathology in CA3 of heterozygous mPS1 mice at 15 months of age. *H–J*, Congo red staining without (*H*) or with (*I, J*) polarizing filters; *K*, Thioflavin T; and *L*, Gallyas silver-staining. *M* and *N*, immunoreactivity in CA3 of wPS1 (*M*) and heterozygous mPS1 mice (*N*) at 16 months of age. *M* and *N*, double immunolabeling with α-tubulin (*red*) and PS199 (*green*) antibodies. *O*, TUNEL staining of dentate gyrus in the wPS1 mouse; *P*, TUNEL staining of dentate gyrus in the homozygous mPS1 mouse; *Q*, TUNEL staining of CA3 in the wPS1 mouse; *R*, TUNEL staining of CA3 in the homozygous mPS1 mouse. Scale bars: 50 μm in *A–F* and *O–R*; 100 μm in *G*; 10 μm in *H–L*; 25 μm in *M* and *N*.

Antibodies—The following antibodies were used: mouse monoclonal anti-tubulin (DM1A, Sigma); anti-ubiquitin (Santa Cruz Biotechnology); anti-GSK3β (Transduction Laboratory); anti-MAP2 (HM2, Sigma); anti-tau Alz50, which recognizes the conformational epitope of paired helical filaments (PHFs), component of NFT (a generous gift from Dr. P. Davies, Albert Einstein College of Medicine, Bronx, NY); anti-phosphorylated tau AT8 (Innogenetics Zwijndrecht); anti-dephosphorylated tau, Tau-1 (Chemicon); rabbit polyclonal anti-tau JM (20); anti-phosphorylated tau PS199, PS262, PS396, PS404, and PS422 (BIOSOURCE), which recognize tau phosphorylated at the indicated sites; and anti-GSK3β Ser-9 (Cell Signaling).

Western Blot Analysis—Brains were homogenized in modified radioimmunoprecipitation assay (RIPA) buffer (50 mM Tris, 150 mM NaCl, 1% Nonidet P-40, 5 mM EDTA, 0.5% sodium deoxycholate, and 0.1% SDS, pH 8.0), and the suspension was centrifuged at 100,000 × *g* for 20 min at 4 °C in an Optima TL ultracentrifuge (Beckman). The pellet was washed five times with 1% SDS-Tris-buffered saline (TBS) (50 mM Tris, 150 mM NaCl, and 1% SDS, pH 8.0) followed each time by centrifugation. The SDS-insoluble pellet was solubilized in 70% formic acid, lyophilized, reconstituted in Laemmli SDS-PAGE sample buffer, and subjected to SDS-PAGE. Separated proteins were blotted onto Immobilon-P membranes (Millipore). The membranes were incubated with primary antibody then with the species-appropriate horseradish peroxidase-conjugated secondary antibody. Immunoreactivity was visualized with a chemiluminescent detection system (ECL, Amersham Biosciences). Quantitation and visual analysis of immunoreactivity were performed with a computer-linked LAS-1000 Bio-Imaging Analyzer System (Fujifilm) using the software program Image Gauge 3.0 (Fujifilm).

Glycogen Synthase Kinase (GSK)-3β Activity—Brains were homogenized in TBS (pH 7.4) and centrifuged at 100,000 × *g* for 20 min at 4 °C in an Optima TL ultracentrifuge (Beckman). Protein concentration in the supernatant was determined with a Bradford protein assay, and 10-μg samples were assayed for GSK-3β activity with an immunoprecipitation assay (21).

Ultrastructural Studies—For electron microscopy studies, SDS-insoluble materials were prepared from the brains of mPS1 mice as described above in the Western blot analysis section. The materials were mildly sonicated and dispersed in phosphate-buffered saline. The dispersed solution was absorbed onto glow-discharged supporting membranes on 400-mesh grids and prefixed by floating the grids on drops of 4% paraformaldehyde in 0.1 M phosphate buffer for 5 min. After washing, the grids were incubated with primary antibody (JM, anti-tau antibody), followed with a 5-nm colloidal gold-conjugated secondary antibody. The grids were then negatively stained with 2% sodium phosphotungstic acid, dried, and observed with a LEO 912AB electron microscope at 100 kV.

Immunohistochemical and Histopathological Studies—Brains were immersion-fixed in 10%-buffered formalin, and paraffin-embedded sections (4 μm) were prepared. PS199, Alz50, anti-MAP2, and AT8 were used as primary antibodies. After reacting the sections with species-appropriate secondary antibodies, we visualized for light microscopy analyses immunoreactive elements by treating the sections with ABC followed by DAB using Peroxidase Stain DAB kits (Nacalai Tesque Japan). PS199 and anti-α-tubulin were used as primary antibodies for confocal laser microscopy analyses. Immunoreactive elements were visualized with Alexa568-conjugated anti-mouse IgG and Alexa488-conjugated anti-rabbit IgG, and then examined with a Radiance 2000 KR3 confocal microscope (Bio-Rad). We stained some sections with Congo red and Thioflavin T, which recognize the β-sheet structure of tau fibrils, and then examined them with a light microscope equipped with crossed polarizing filters (Nikon). NFTs were identified using a standard Gallyas silver-impregnation method, which is used to assess structural changes of the brain in AD (22).

RESULTS

The Aβ levels in the brains of mPS1 knock-in mice were quantified by sandwich enzyme-linked immunoassay (23) and Western blot analysis. Similar to a previous report (19), the level of $A\beta_{1-42}$ was elevated in the brains of mPS1 mice compared with that in the brains of wild-type mice (wPS1 mice). Most of the $A\beta_{1-40}$ and $A\beta_{1-42}$ was recovered in the Triton X-100-soluble fraction, and very little was recovered in the 1% SDS-insoluble fraction, suggesting that neither $A\beta_{1-40}$ nor $A\beta_{1-42}$ aggregated and deposited within the brains of the mPS1 mice. Moreover, Aβ immunostaining in tissue sections was absent, suggesting again that neither extracellular nor intracellular Aβ accumulated *in vivo* (data not shown). Thus, murine Aβ failed to deposit in the brains of mPS1 mice, even though $A\beta_{1-42}$ levels in these brains increased.

Characterization of NFT-like Pathology in Mutant PS1 Mice—Five-month-old heterozygous mPS1 mice exhibited no pathological changes (Fig. 1*A*); however, in 7-month-old or older mice, we detected phospho-tau accumulation (PS199) in neurons in the hippocampal region (Fig. 1*B*). The prevalence and distribution of these PS199-positive neurons gradually increased and widened, respectively, with age, and in 14–16-month-old mice, we observed phospho-tau immunoreactivity in hippocampal CA3 neurons (Fig. 1*D*). By contrast, wPS1 mice did not show this pattern of phospho-tau immunoreactivity (Fig. 1, *C* and *D*). Alz50, an antibody that recognizes the conformational change of tau in PHF-tau, also labeled CA3 neurons (Fig. 1, *E–G*). In summary, these findings indicate that heterozygous mPS1 mice, whose alleles most precisely reflect the genotype of humans bearing this mutation, exhibited phospho-tau accumulation with PHF-tau epitopes, whereas wPS1 mice of the same age showed no sign of tau accumulation.

Data related to the other histological criteria for NFTs confirmed these findings. In heterozygous mPS1 mice, we observed Congo red birefringence (Fig. 1, *H–J*) and Thioflavin T reactivity (Fig. 1*K*) in hippocampal neurons. The Gallyas silver staining method revealed argyrophillic neurons in the hippocampus of mPS1 mice (Fig. 1*L*). Argyrophillic and Congo red-positive neurons were less numerous than phospho-tau-positive neurons (less than 5% of phospho-tau-positive neurons). The tau-accumulating neurons of these mice also exhibited reduced α-tubulin immunoreactivity (Fig. 1, *M* and *N*) similar to that displayed by NFT-bearing neurons. As we previously showed in tau Tg mice (24, 25), weaker α-tubulin immunoreactivity might indicate destruction of microtubules in tau-accumulating neurons in the mPS1 mice. TUNEL staining, however, revealed no signs of apoptosis in these neurons (Fig. 1, *O–R*). Taken together, these results suggest that mPS1 affects the cytoskeleton of hippocampal neurons and induces NFT-like accumulation of hyperphosphorylated tau.

Biochemical and Ultrastructural Analysis of Tau in Mutant PS1 Mice—We confirmed the accumulation of NFT-like tau in mPS1 mice with biochemical and electron microscopy analyses. Because tau becomes detergent insoluble when aggregated, we assessed the amount of tau in the SDS-insoluble fraction derived from the brains of mPS1 mice. As shown in Fig. 2*A*, small amounts of tau were recovered in the SDS-insoluble fraction from 2-month-old mPS1 mice. The amount of tau recovered in the SDS-insoluble fraction increased with aging, and a large amount of tau was recovered from 14-month-old heterozygous mPS1 mice compared with age-matched wPS1 mice. (The amount of SDS-insoluble tau in mPS1 mice was ~2% of the total tau in these mice).

We also investigated the amount of SDS-insoluble tau in different brain regions of mPS1 mice. Tau was recovered from the hippocampus, and small amounts were recovered from the cerebral cortex, striatum, and cerebellum. This might be explained by the inverse correlation of NFT with pin1 expression (26).

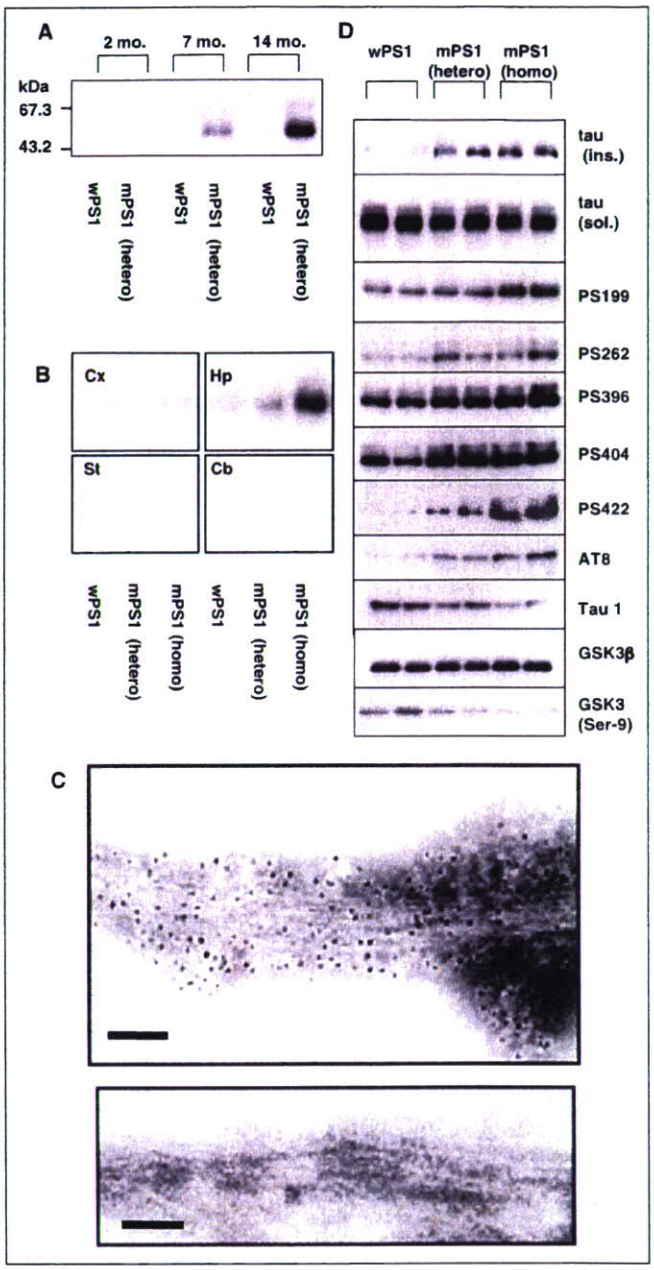

FIGURE 2. **Biochemical and electron microscopy (EM) analyses of mPS1 mice.** *A*, SDS-insoluble tau from the brains of 2-, 7-, and 14-month-old heterozygous mPS1 mice. *B*, SDS-insoluble tau in micro-dissected cortex (*Cx*), hippocampus (*Hp*), brainstem (*St*), and cerebellum (*Cb*) of 12-month-old wild-type PS1, heterozygous mPS1, and homozygous mPS1 mice. *C*, immuno-EM analysis of SDS-insoluble materials from 12-month-old heterozygous mPS1 mice. Fibrils labeled with 5-nm gold particles indicate immunoreactivity to the phosphorylation-independent tau antibody, JM (*upper panel*). Immunogold labeling was not observed on fibrils (*control*) stained in the absence of primary antibody (*lower panel*). Scale bars: 100 nm. *D*, Western blots containing SDS-insoluble and RIPA-soluble materials from the hippocampi of 14-month-old w wPS1, heterozygous mPS1, and homozygous mPS1 mice. (Lane pairs correspond to a set of two mice per mouse strain.) Order of blots (from *top* to *bottom*): SDS-insoluble tau (*tau (ins.)*); RIPA-soluble tau (*tau (sol.)*); RIPA-soluble phosphorylated tau (*PS199, PS262, PS396, PS404, PS422,* and *AT8*); unphosphorylated tau (*Tau1*), active GSK3β (*GSK3β*); and inactive GSK3β (*GSK3β (Ser-9)*).

The SDS-insoluble material recovered from mPS1 mice were further investigated with electron microscopy. As shown in Fig. 2*C*, tau-positive fibrils were detected in the SDS-insoluble fraction. These fibrils appeared to be straight tubules, about 10 nm in diameter. The biochem-

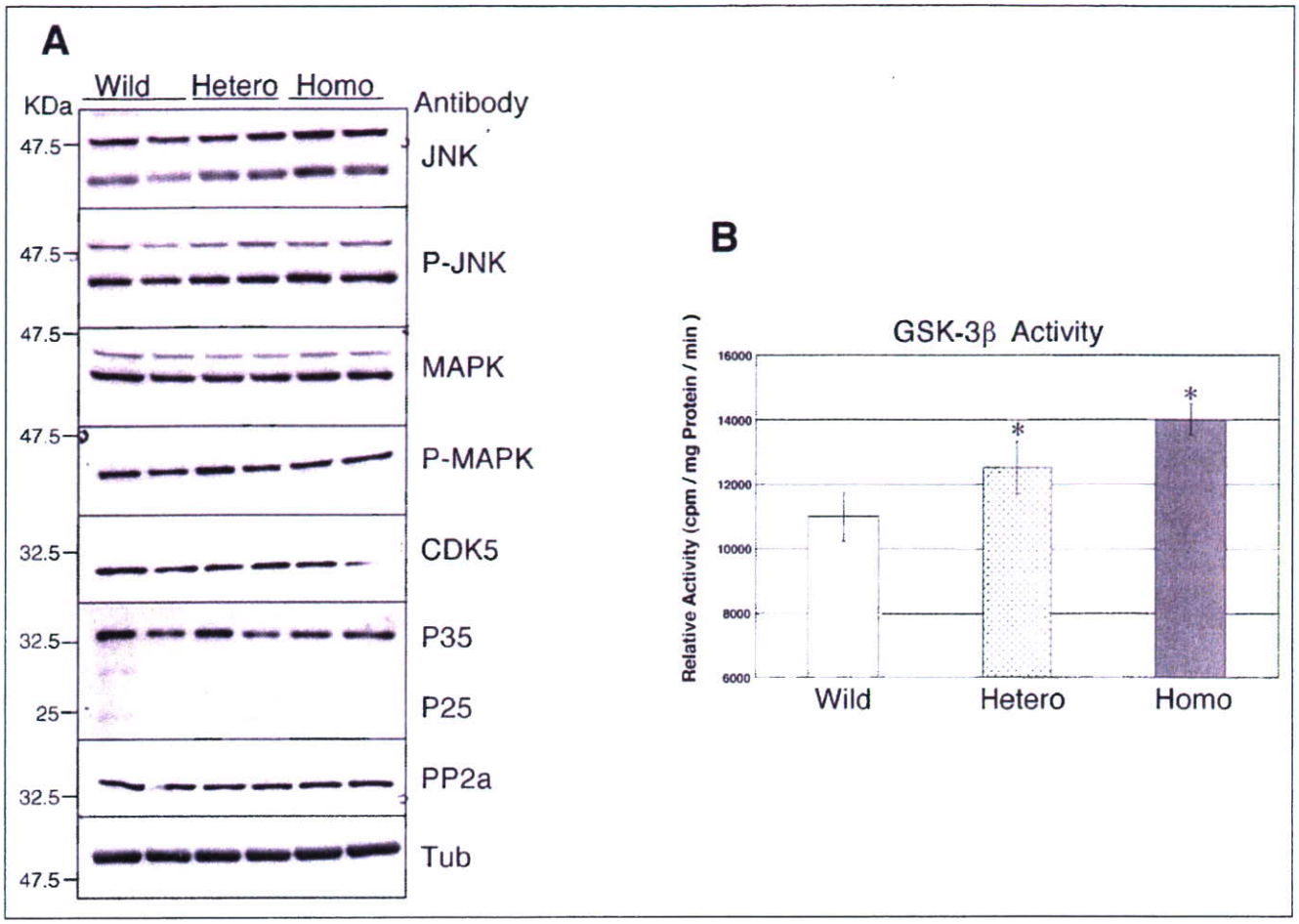

FIGURE 3. **Tau kinase activity in 12-month-old mPS1 mice.** *A*, hippocampal lysates from wPS1, heterozygous mPS1, and homozygous mPS1 mice were analyzed with Western blotting and antibodies against tau kinases and phosphatases: total JNK (*JNK*); phospho-JNK (*P-JNK*); MAP kinase (*MAPK*); phosphorylated MAP kinase (*PMAPK*); CDK5; the CDK5 activators, p35 and p25; and phosphatase 2a (*PP2a*)). A blot stained with anti-tubulin antibody (*Tub*) represents the control. *B*, GSK-3β activity in immunoprecipitated brain samples derived from wPS1, heterozygous mPS1, and homozygous mPS1 mice were determined with an assay that measures the incorporation of ^{32}P into a GSK-3β substrate peptide. Data are expressed as averages ± S.D. (*, $p < 0.05$; $n = 3$).

ical and ultrastructural analyses strongly suggest that NFT-like tau aggregation formed primarily in hippocampal neurons of mPS1 mice.

The NFTs found in AD brains contain highly phosphorylated tau (27). Hyperphosphorylation of tau leads to the formation of fibrillar tau (28). To determine whether tau hyperphosphorylation also occurs in mPS1 mice, we examined the extent of tau phosphorylation in 14-month-old wPS1, heterozygous mPS1, and homozygous mPS1 mice (Fig. 2*D*). Immunoblotting with various phosphorylation-dependent anti-tau antibodies revealed that the amount of SDS-insoluble tau was nearly the same in heterozygous and homozygous mPS1 mice (Fig. 2*D*, *tau(ins.)*). This amount, however, was greater than that in wPS1 mice. Although the total amounts of tau in soluble fractions from the three types of mice were similar (*i.e.* bands had slower mobility than the unphosphorylated Tau-1-immunoreactive band) (Fig. 2*D*, *tau(sol.)*), the amounts of phosphorylated tau immunostained by PS199, PS262, PS396, PS404, PS422, and AT8 were elevated in the heterozygous and homozygous mPS1 mice compared with those in the wPS1 mice. The extent of tau phosphorylation at the AT8, PS422, and PS199 epitopes appeared to depend on the number of mPS1 alleles present in the mice, as shown by the comparatively greater immunosignal intensity of samples derived from homozygous than in heterozygous mPS1 mice, suggesting that mPS1 expression affects the hyperphosphorylation of tau. The immunostaining intensity of Tau-1, an antibody that recognizes unphosphorylated tau, also correlated with genotype. Tau-1 immunoreactivity was greater in samples derived from wPS1 mice than in heterozygous and homozygous mPS1 mice (wPS1 > heterozygous mPS1 > homozygous mPS1), confirming that mPS1 induced the hyperphosphorylation of tau.

GSK-3β, Tau Kinase, and Tau Phosphatase Activity—Activation of GSK-3β, a known tau kinase, was also associated with mPS1 genotype. Although total GSK-3β levels were similar among wPS1, heterozygous mPS1, and homozygous mPS1 mice, inactive GSK-3β (GSK-3β phosphorylated at Ser-9) levels varied inversely with the number of mPS1 alleles present (Fig. 2*D*; GSK3β and GSK3β(*Ser-9*)). This inverse correlation was confirmed by comparing the GSK-3β activity in immunoprecipitated brain samples derived from wPS1, heterozygous mPS1, and homozygous mPS1 mice (Fig. 3*B*). This assay revealed elevated GSK-3β activity in heterozygous mPS1 compared with wPS1 mice ($p < 0.05$; $n = 3$), and also in homozygous mPS1 mice compared with heterozygous mice ($p < 0.05$; $n = 3$). Taken together, we conclude that the mutant PS1 activated GSK-3β, thereby enhancing tau phosphorylation and resulting in the formation of NFT-like tau aggregates (Figs. 1 and 2). These results support those from a previous report (20).

We also investigated how other kinases and phosphatases may contribute to tau phosphorylation in mPS1 mice. As shown in Fig. 3*A*, levels of the active forms of phosphorylated JNK; phosphorylated MAP kinase; CDK5;

the CDK5 activators p35 and p25; and PP2a were similar among wPS1, heterozygous mPS1, and homozygous mPS1 mice, indicating that the tau phosphorylation mediated by these enzymes are not affected by the PS1 mutation. Nonetheless, other mechanisms are expected to be involved in the mPS1-induced hyperphosphorylation of tau, because GSK-3β alone cannot phosphorylate all of the phosphorylation sites in tau.

DISCUSSION

In the present study, we demonstrated that the brains of mice harboring a PS1 mutation accumulated NFT-like phospho-tau. Biochemical analysis of SDS-insoluble tau revealed tau fibrils. These NFT-like tau inclusions were similar to those observed in FTDP-17 mutant tau transgenic mice (24, 25, 28), in mice overexpressing p25, a CDK5 activator (29), and in Pin1 knock-out mice (26). The neurons of other PS1 knock-in and mutant PS1 transgenic mice; however, failed to show cytoskeletal changes (30, 31). To create their mutant PS1 knock-in mice, Guo *et al.* (32) used a hybrid mouse composed of 129SV and C57BL6 strains, whereas in the present study we used mice resulting from 10 generations of crossbreeding with C57BL6J mice. The genetic background of our mice, which is most likely to be different from the backgrounds of mice used in previously studies, could have influenced how the PS1 mutation contributed to NFT formation and cytoskeletal changes. Another possible explanation for the apparent discrepancy between our findings and others is that our PS1 knock-in mice harbored a different PS1 mutation from that harbored by mutant PS1 knock-in mice developed by other laboratories.

Previously, we found certain PS1 mutations that increase $A\beta_{1-42}$ levels are poor predictors for the onset of FAD (5). Our present results, however, suggest that the accumulation of NFT-like tau could determine the onset of AD. These two differing outcomes would also explain why some PS1 mutations accelerate NFT formation and neuronal loss without accelerating Aβ deposition (18). Thus, PS1 mutations that accelerate both NFT formation and $A\beta_{1-42}$ production may further accelerate related neuropathologies, suggesting that the cause of early onset AD may be related to a PS1 mutation.

The mechanism underlying the mutant PS1-associated accumulation of NFTs may involve the activation of GSK-3β. Our results indicate that GSK-3β is activated in our mPS1 knock-in mice; this is consistent with other mPS1 transgenic mice. Recently, wild-type PS1 has been shown to activate PI3 kinase/Akt signaling by promoting the association of cadherin and PI 3-kinase, whereas mutant PS1 was unable to do so (32). Thus, mutant PS1 appears to impair PI 3-kinase/Akt signaling by affecting selected signaling receptors (33) or by reducing cadherin/PI3 kinase association (32), which eventually leads to the activation of GSK-3β. Whereas the mutant PS1-associated activation of GSK-3β occurred in young mice, tau accumulation occurred only later on in older mice. This led us to hypothesize that, by some mechanism, phosphorylated tau degrades before it aggregates. This unknown mechanism is then inactivated during aging, leading to the accumulation and aggregation of tau that occurs in aged individuals.

Patients harboring the FAD mutation of PS1 develop AD with 100% penetration. Based on our results, we propose that the PS1 mutation in FAD leads to the early onset of AD through the activation of GSK-3β, which leads to NFT formation and the loss of neurons and synapses. Moreover, we believe that the rate of GSK-3β activation is accelerated by extracellular Aβ oligomers. The exact molecular mechanism mediating the mutant PS1-induced activation of GSK-3β requires clarification to further our understanding of how AD develops.

REFERENCES

1. Sherrington, R., Rogaev, E. I., Liang, Y., Rogaeva, E. A., Levesque, G., Ikeda, M., Chi, H., Lin, C., Li, G., Holman, K., Tsuda, T., Mar, L., Foncin, J.-F., Bruni, A. C., Montesi, M. P., Sorbi, S., Rainero, I., Pinessi, L., Nee, L., Chumakov, I., Pollen, D., Brookes, A., Sanseau, P., Polinsky, R. J., Wasco, W., Da Silva, H. A. R., Haines, J. L., Pericak-Vance, M. A., Tanzi, R. E., Roses, A. D., Fraser, P. E., Rommens, J. M., and St. George-Hyslop, P. H. (1995) *Nature* **375,** 754–760
2. Cruts, M., Backhovens, H., Wang, S. Y., Van Gassen, G., Theuns, J., De Jonghe, C. D., Wehnert, A., De Voecht, J., De Winter, G., and Cras, P. (1995) *Hum. Mol. Genet.* **4,** 2363–2371
3. St George-Hyslop, P. H., and Petit, A. (2005) *C. R. Biol.* **328,** 119–130
4. St George-Hyslop, P. H. (2000) *Biol. Psychiatry* **47,** 183–199
5. Murayama, O., Honda, T., Mercken, M., Murayama, M., Yasutake, K., Nihonmatsu, N., Nakazato, Y., Michel, G., Song, S., Sato, K., Takahashi, H., and Takashima, A. (1997) *Neurosci. Lett.* **229,** 61–64
6. Scheuner, D., Eckman, C., Jensen, M., Song, X., Citron, M., Suzuki, N., Bird, T. D., Hardy, J., Hutton, M., Kukull, W., Larson, E., Levy-Lahad, E., Viitanen, M., Peskind, E., Poorkaj, P., Schellenberg, G., Tanzi, R., Wasco, W., Lannfelt, L., Selkoe, D., and Younkin, S. (1996) *Nat. Med.* **2,** 864–870
7. Holcomb, L., Gordon, M. N., McGowan, E., Yu, X., Benkovic, S., Jantzen, P., Wright, K., Saad, I., Mueller, R., Morgan, D., Sanders, S., Zehr, C., O'Campo, K., Hardy, J., Prada, C. M., Eckman, C., Younkin, S., Hsiao, K., and Duff, K. (1998) *Nat. Med.* **4,** 97–100
8. Chang, P., and Su, Y. (2000) *Brain Res. Brain Res. Protoc.* **6,** 6–12
9. Klein, A. M., Kowall, N. W., and Ferrante, R. J. (1999) *Ann. N. Y. Acad. Sci.* **893,** 314–320
10. Morelli, L., Prat, M. I., and Castano, E. M. (1999) *Cell Tissue Res.* **298,** 225–232
11. Butterfield, D. A. (2002) *Free Radic. Res.* **36,** 1307–1313
12. Yu, H., Saura, C. A., Choi, S. Y., Sun, L. D., Yang, X., Handler, M., Kawarabayashi, T., Younkin, L., Fedeles, B., Wilson, M. A., Younkin, S., Kandel, E. R., Kirkwood, A., and Shen, J. (2001) *Neuron* **31,** 713–726
13. Amtul, Z., Lewis, P. A., Piper, S., Crook, R., Baker, M., Findlay, K., Singleton, A., Hogg, M., Younkin, L., Younkin, S. G., Hardy, J., Hutton, M., Boeve, B. F., Tang-Wai, D., and Golde, T. E. (2002) *Neurobiol. Dis.* **9,** 269–273
14. Dermaut, B., Kumar-Singh, S., Engelborghs, S., Theuns, J., Rademakers, R., Saerens, J., Pickut, B. A., Peeters, K., van den Broeck, M., Vennekens, K., Claes, S., Cruts, M., Cras, P., Martin, J. J., Van Broeckhoven, C., and De Deyn, P. P. (2004) *Ann. Neurol.* **55,** 617–626
15. Tang-Wai, D., Lewis, P., Boeve, B., Hutton, M., Golde, T., Baker, M., Hardy, J., Michels, V., Ivnik, R., Jack, C., and Petersen, R. (2002) *Dement. Geriatr. Cogn. Disord.* **14,** 13–21
16. Evin, G., Smith, M. J., Tziotis, A., McLean, C., Canterford, L., Sharples, R. A., Cappai, R., Weidemann, A., Beyreuther, K., Cotton, R. G., Masters, C. L., and Culvenor, J. G. (2002) *Neuroreport* **13,** 719–723
17. Yoshiyama, Y., Lee, V. M., and Trojanowski, J. Q. (2001) *Curr. Neurol. Neurosci. Rep.* **1,** 413–421
18. Gomez-Isla, T., Growdon, W. B., McNamara, M. J., Nochlin, D., Bird, T. D., Arango, J. C., Lopera, F., Kosik, K. S., Lantos, P. L., Cairns, N. J., and Hyman, B. T. (1999) *Brain* **122,** 1709–1719
19. Nakano, Y., Kondoh, G., Kudo, T., Imaizumi, K., Kato, M., Miyazaki, J. I., Tohyama, M., Takeda, J., and Takeda, M. (1999) *Eur. J. Neurosci.* **11,** 2577–2581
20. Takashima, A., Murayama, M., Murayama, O., Kohno, T., Honda, T., Yasutake, K., Nihonmatsu, N., Mercken, M., Yamaguchi, H., Sugihara, S., and Wolozin, B. (1998) *Proc. Natl. Acad. Sci. U. S. A.* **95,** 9637–9641
21. Van Lint, J., Khandelwal, R. L., Merlevede, W., and Vandenheede, J. R. (1993) *Anal. Biochem.* **208,** 132–137
22. Iqbal, K., Braak, E., Braak, H., Zaidi, T., and Grundke-Iqbal, I. (1991) *Neurobiol. Aging* **12,** 357–361
23. Sun, X., Cole, G. M., Chu, T., Xia, W., Galasko, D., Yamaguchi, H., Tanemura, K., Frautschy, S. A., and Takashima, A. (2002) *Neurobiol. Aging* **23,** 195–203
24. Tatebayashi, Y., Miyasaka, T., Chui, D. H., Akagi, T., Mishima, K., Iwasaki, K., Fujiwara, M., Tanemura, K., Murayama, M., Ishiguro, K., Planel, E., Sato, S., Hashikawa, T., and Takashima, A. (2002) *Proc. Natl. Acad. Sci. U. S. A.* **99,** 13896–13901
25. Tanemura, K., Murayama, M., Akagi, T., Hashikawa, T., Tominaga, T., Ichikawa, M., Yamaguchi, H., and Takashima, A. (2002) *J. Neurosci.* **22,** 133–141
26. Liou, Y. C., Sun, A., Ryo, A., Zhou, X. Z., Yu, Z. X., Huang, H. K., Uchida, T., Bronson, R., Bing, G., Li, X., Hunter, T., and Lu, K. P. (2003) *Nature* **424,** 556–561
27. Lee, V. M., Balin, B. J., Otvos, L., Jr., and Trojanowski, J. Q. (1991) *Science* **251,** 675–678
28. Sato, S., Tatebayashi, Y., Akagi, T., Chui, D. H., Murayama, M., Miyasaka, T., Planel, E., Tanemura, K., Sun, X., Hashikawa, T., Yoshioka, K., Ishiguro, K., and Takashima, A. (2002) *J. Biol. Chem.* **277,** 42060–42065
29. Cruz, J. C., Tseng, H. C., Goldman, J. A., Shih, H., and Tsai, L. H. (2003) *Neuron* **40,** 471–483
30. Siman, R., Reaume, A. G., Savage, M. J., Trusko, S., Lin, Y. G., Scott, R. W., and Flood, D. G. (2000) *J. Neurosci.* **20,** 8717–8726
31. Guo, Q., Sebastian, L., Sopher, B. L., Miller, M. W., Ware, C. B., Martin, G. M., and Mattson, M. P. (1999) *J. Neurochem.* **72,** 1019–1029
32. Baki, L., Shioi, J., Wen, P., Shao, Z., Schwarzman, A., Gama-Sosa, M., Neve, R., and Robakis, N. K. (2004) *EMBO J.* **23,** 2586–2596
33. Kang, D. E., Sang Yoon, I., Repetto, E., Busse, T., Yermian, N., Ie, L., and Koo, E. H. (2005) *J. Biol. Chem.* **280,** 31537–31547

Indispensability of the glutamate transporters GLAST and GLT1 to brain development

Toshiko R. Matsugami*†, Kentaro Tanemura‡§, Michihiro Mieda*, Reiko Nakatomi†, Keiko Yamada¶, Takashi Kondo‡, Masaharu Ogawa‖, Kunihiko Obata**, Masahiko Watanabe¶, Tsutomu Hashikawa†,††, and Kohichi Tanaka*†††‡‡

*Laboratory of Molecular Neuroscience, School of Biomedical Science and Medical Research Institute, Tokyo Medical and Dental University, 1-5-45 Yushima, Bunkyo-ku, Tokyo 113-8510, Japan; †Laboratory for Neural Architecture, ‡Brain Development Research Group, ‖Laboratory for Cell Culture Development, and **Neuronal Circuit Mechanisms Research Group, RIKEN Brain Science Institute, 2-1 Hirosawa, Wako-shi, Saitama 351-0198, Japan; ¶Department of Anatomy, Hokkaido University Graduate School of Medicine, Sapporo 060-8638, Japan; and ‡‡Precursory Research for Embryonic Science and Technology, Japan Science and Technology Corporation, 4-1-8 Hon-cho, Kawaguchi, Saitama 332-0012, Japan

Edited by Michael V. L. Bennett, Albert Einstein College of Medicine, Bronx, NY, and approved June 22, 2006 (received for review October 19, 2005)

Previous *in vitro* studies have shown that the neurotransmitter glutamate is important in brain development. Paradoxically, loss-of-function mouse models of glutamatergic signaling that are generated by genetic deletion of glutamate receptors or glutamate release show normal brain assembly. We examined the direct consequences on brain development of extracellular glutamate buildup due to the depletion of the glutamate transporters GLAST and GLT1. GLAST/GLT1 double knockout mice show multiple brain defects, including cortical, hippocampal, and olfactory bulb disorganization with perinatal mortality. Here, we report abnormal formation of the neocortex in GLAST/GLT1 mutants. Several essential aspects of neuronal development, such as stem cell proliferation, radial migration, neuronal differentiation, and survival of SP neurons, were impaired. These results provide direct *in vivo* evidence that GLAST and GLT1 are necessary for brain development through regulation of extracellular glutamate concentration and show that an important mechanism is likely to be maintenance of glutamate-mediated synaptic transmission.

axon/dendrite development | cortex | radial fiber

Neuronal activity is important in the process of refining neural connections in the developing brain (1). Activity, however, may also act to influence earlier developmental events, such as proliferation, migration, differentiation, and survival (2, 3). As key mediators of neuronal activity, neurotransmitters released by neuronal activity are thought to have important signaling roles in shaping the early development of the CNS (3). Previous observations suggest that the major excitatory neurotransmitter, glutamate, provides important communication signals in the developing brain. Indeed, glutamate has been shown to modulate cell proliferation, radial migration, neuronal survival linked to apoptosis, and neuronal differentiation (4–7). In contrast to these observations, most studies in which glutamatergic activity was blocked, whether at the level of ligand or receptor, have demonstrated little, if any, developmental defects (8–14). Thus, according to *in vivo* experiments using loss-of-function models, early glutamate signaling appears to be dispensable. However, because compensatory mechanisms, coupled with a redundancy in glutamate receptor mechanisms, could reduce the severity of a brain phenotype in loss-of-function models, glutamate may still play a role at an early stage of brain development. To investigate this issue, we generated a genetically manipulated animal in which glutamate receptors are overstimulated by genetic deletion of glutamate transporters. Glutamate transporters are essential for the maintenance of low extracellular levels of glutamate (15). The glutamate transporters GLAST, GLT1, and EAAC1 are expressed in the embryonic mouse CNS (16). Previous studies demonstrated that mice lacking GLAST, GLT1, or EAAC1 have seemingly normal brain development (17–19). These results raised the possibility that glutamate transporter subtypes can functionally substitute for one another in CNS development. In the present study, we inactivated two members of the glutamate transporter family to elucidate roles of the glutamate system in CNS development.

Results

GLAST$^{-/-}$/GLT1$^{-/-}$ Mutants Have Multiple Brain Defects. Normal development of the CNS was observed in mutant mice lacking GLAST/EAAC1 or EAAC1/GLT1 (data not shown). By contrast, mice lacking GLAST/GLT1 died *in utero* [around embryonic days (E17–18)] and exhibited abnormal brain development after E15 (Fig. 1; see also Figs. 8 and 9, which are published as supporting information on the PNAS web site). The lateral ventricles in GLAST$^{-/-}$/GLT1$^{-/-}$ mice were dilated relative to those in control mice, and alterations in the structure of the pallial–subpallial boundary were observed in the mutant mice (Fig. 1 *A–D*).The E16 neocortex is laminated, with the following layers: marginal zone, cortical plate (CP), subplate (SP), intermediate zone, and ventricular zone (VZ) (Fig. 1*E*). In the GLAST$^{-/-}$/GLT1$^{-/-}$ mutants, the CP border on the intermediate zone was obscured, and the SP could not be identified (Fig. 1*F*). In addition, cell number in the VZ was decreased in mutant brains (23,558.3 ± 111.6 cells per mm^2 for WT; 20,216.6 ± 119.7 cells per mm^2 for the double mutant; $n = 4$; $P < 0.0001$; Fig. 1 *E* and *F*). Moreover, there were distortions in the organization of the hippocampus and the olfactory bulb of GLAST$^{-/-}$/GLT1$^{-/-}$ mice (Fig. 8). In the hippocampus, pyramidal neurons were less densely packed. In the olfactory bulb of GLAST$^{-/-}$/GLT1$^{-/-}$ mice, the mitral cell layer was absent. The present study focused on the cortical malformation of GLAST$^{-/-}$/GLT1$^{-/-}$ mice.

Expression of GLT1 and GLAST in the Embryonic Brain. GLAST is an astrocytic glutamate transporter in the adult CNS (20). Previous immunocytochemical studies have shown that GLT1 is strongly expressed, primarily by astrocytes, in the adult brain (20). However, we have recently demonstrated that GLT1 is also expressed by some neurons in the hippocampus (21). Because the two transporters show dynamic changes in expression during CNS development (16), we examined cellular elements expressing the two transporters in the embryonic cortex of C57BL mice by immunohistochemistry with subtype-specific antibodies. At

Conflict of interest statement: No conflicts declared.

This paper was submitted directly (Track II) to the PNAS office.

Freely available online through the PNAS open access option.

Abbreviations: E*n*, embryonic day *n*; PCNA, proliferating cell nuclear antigen; MAP2, microtubule-associated protein 2; CT, corticothalamic; TC, thalamocortical; DiI, 1,1′-dioctadecyl-3,3,3′,3′-tetramethylindocarbocyanine; AMPA, α-amino-3-hydroxy-5-methyl-4-isoxazolepropionic acid; VZ, ventricular zone; CP, cortical plate; SP, subplate.

§Present address: Cellular and Molecular Toxicology Division, National Institute of Health Sciences, 1-18-1 Kamiyoga, Setagayaku, Tokyo 158-8501, Japan.

††To whom correspondence may be addressed. E-mail: tom@brain.riken.jp or tanaka.aud@mri.tmd.ac.jp.

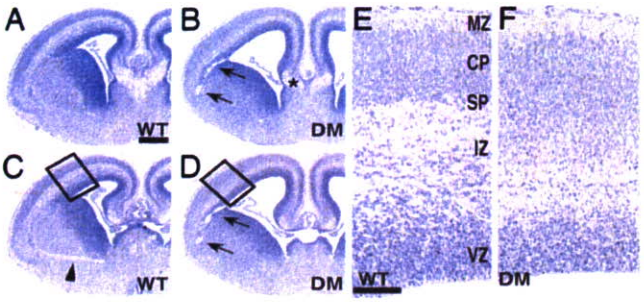

Fig. 1. Morphological abnormalities in brains of GLAST$^{-/-}$/GLT1$^{-/-}$ mutants. Coronal sections of whole brain (*A–D*) and neocortex (*E* and *F*) at E16 from WT (*A*, *C*, and *E*) and GLAST$^{-/-}$/GLT1$^{-/-}$ double mutant (DM) (*B*, *D*, and *F*) embryos stained with hematoxylin. Images in *A* and *B* are located anterior to those in *C* and *D*. Boxed regions in *C* and *D* are enlarged in *E* and *F*, respectively. The corpus callosum did not cross the midline, and a Probst bundle (asterisk in *B*) was formed. Arrowhead in *C* indicates the anterior commissure, which was absent in GLAST$^{-/-}$/GLT1$^{-/-}$ mutants. Delamination of the pallial–subpallial junction can be seen in the region between arrows in *B* and *D*. MZ, marginal zone; IZ, intermediate zone. (Scale bars: *A*, 500 μm; *E*, 100 μm.)

E16, GLT1 was expressed in the globus pallidus, perirhinal cortex, lateral hypothalamus, hippocampus, and fimbria and in the axonal pathways interconnecting the neocortex, basal ganglia, and thalamus (Fig. 2 *A* and *C*). In the cerebral cortex, GLT1 immunoreactivity was seen in the SP and along fiber bundles in the intermediate zone (Fig. 2*C*; see also Fig. 10*A*, which is published as supporting information on the PNAS web site). To investigate further the cellular localization of GLT1 in the cortex, we performed double immunostaining of GLT1 with GAP-43 (growth-associated protein 43), a neuronal marker. GLT1 immunoreactivity was double-labeled by GAP-43, suggesting that GLT1 was expressed in neurons at E16 (Fig. 10). In contrast, GLAST protein was expressed in radial glial cells in the VZ of telencephalon and diencephalon at E16 (Fig. 2 *B* and *D*). GLAST immunoreactivity was also found in a palisade of radial glial fibers originating in the VZ near the lateral ganglionic eminence–pallium angle and coursing to the pial surface (Fig. 2*B*). GLT1 and GLAST are thus localized during development on neurons and radial glial cells, respectively, suggesting that the two glutamate transporters might play cooperative and complementary roles in neural development (22). Although GLT1 accounts for ≈94% of the total glutamate uptake activity in the adult forebrain (17), both GLAST and GLT1 are major glutamate transporters in the embryonic brain. Therefore, brain development is disturbed in GLAST/GLT1 double knockout mice but not in GLAST or GLT1 knockout mice.

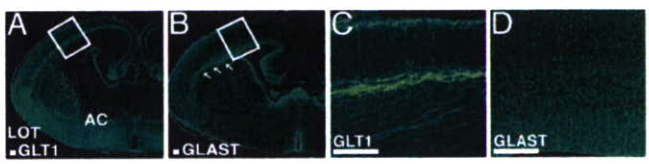

Fig. 2. GLT1 and GLAST immunoreactivity in the mouse forebrain at E16. (*A* and *C*) GLT1 was expressed in the globus pallidus, perirhinal cortex, lateral hypothalamus, hippocampus, and fimbria and the axonal pathways interconnecting the neocortex, basal ganglia, and thalamus. (*B* and *D*) In contrast, strong GLAST immunoreactivity was seen in radial glial cells and the radial glial fascicle. Boxed regions in *A* and *B* are enlarged in *C* and *D*, respectively. Arrows in *B* indicate the radial glial fascicle. AC, anterior commissure; LOT, lateral olfactory tract. (Scale bars: 100 μm.)

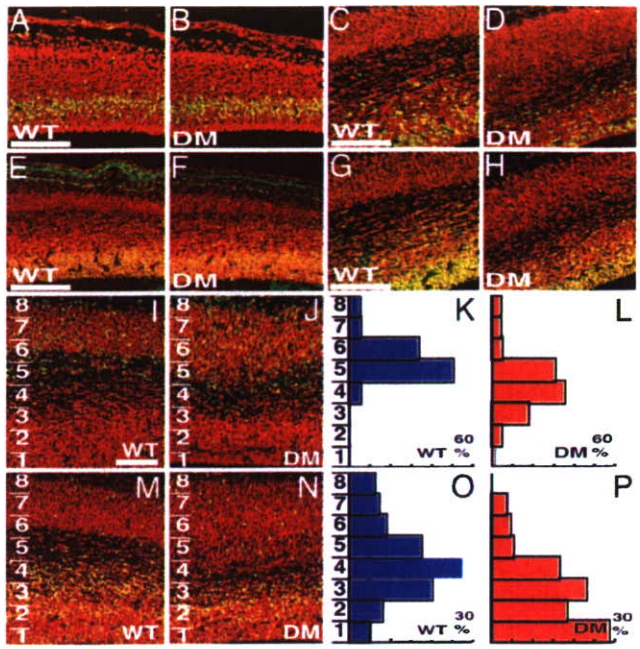

Fig. 3. Reduced cell proliferation and abnormal neural migration in the GLAST$^{-/-}$/GLT1$^{-/-}$ mutant neocortex. Immunoreactivities of BrdU and PCNA are visualized as green fluorescence. (*A–J* and *M* and *N*) All nuclei were counterstained with propidium iodide (PI) (red). Thus, the BrdU- and PCNA-positive cells appear yellow because they are colabeled for PI and BrdU or PCNA. However, some BrdU- and PCNA-positive cells appear green, because green fluorescence is intensified for easy identification of the BrdU- and PCNA-positive cells. There were a comparable number of BrdU-positive cells in WT (*A*) and mutant (*B*) E14 cortices. However, at E16, the number of BrdU-positive cells was reduced in mutant (*D*) compared with WT (*C*) cortex. (*E–H*) PCNA expression at E14 (*E* and *F*) and E16 (*G* and *H*). BrdU was injected at E12 (*I* and *J*) or E14 (*M* and *N*), followed by examination of the distribution of BrdU-positive cells at E16. (*I–P*) To quantify migration, we counted heavily labeled cells (first generation at time of BrdU injection) at E16. The cortices were divided into eight equal areas (numbered 1–8). The percentage of BrdU-positive cells (percentage of total) in each area was determined, and results were plotted as histograms of WT (*K* and *O*) and GLAST$^{-/-}$/GLT1$^{-/-}$ double mutants (DM) (*L* and *P*). (Scale bars: 100 μm.)

Cell Birth and Death in the GLAST$^{-/-}$/GLT1$^{-/-}$ Cortex. A decrease in cell number in the VZ of mutant brains could be caused by reduced cell proliferation or accelerated cell death. To assess the proliferation profile of mutant neuronal progenitors, embryos were pulse-labeled *in utero* with BrdU. At E14, the percentage of BrdU-positive cells in the VZ was similar in WT and mutant mice (25.0 ± 1.7% for WT; 26.0 ± 2.3% for double mutant; n = 6; Fig. 3 *A* and *B*). At E16, however, the percentage of BrdU-positive cells in the VZ was decreased in mutants (18.3 ± 0.3% for WT; 16.2 ± 0.4% for double mutant; n = 4; $P < 0.01$; Fig. 3 *C* and *D*). Proliferation of neuronal progenitor cells was also examined by immunohistochemistry for proliferating cell nuclear antigen (PCNA), a marker of proliferating cells. The pattern of PCNA immunostaining replicated the BrdU results (Fig. 3 *E–H*).This finding is consistent with the results of a previous *in vitro* study that showed that application of glutamate decreased the number of embryonic cortical cells that incorporate BrdU (5). To determine whether cell death was increased in the cortex of double mutants, we used the TUNEL method to stain apoptotic cells. Apoptosis was not increased in the neocortex of mutants at E14 or E16 (data not shown). These results suggest that both GLT1 and GLAST regulate neurogenesis by controlling the extracellular glutamate concentration at E16.

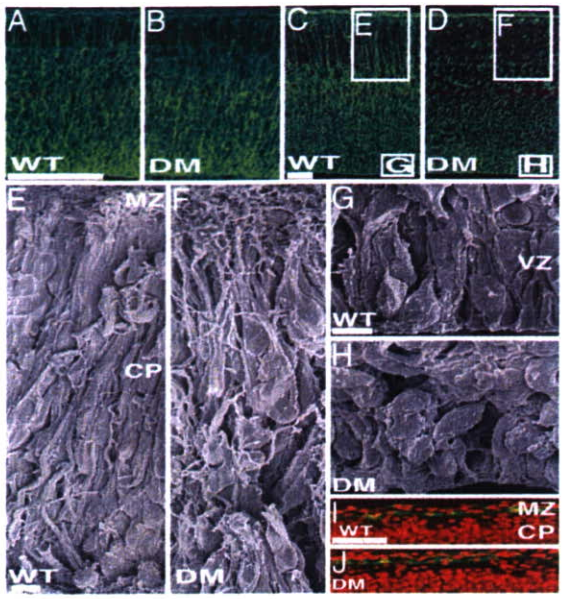

Fig. 4. Altered radial glial systems and normal Reelin expression in GLAST$^{-/-}$/GLT1$^{-/-}$ mutants. (*A–D*) Nestin staining of E14 and E16 cortices. The pattern and distribution of radial glial fibers is comparable in WT (*A*) and double mutant (DM) (*B*) mice at E14. At E16, however, disruption of radial fibers was apparent in mutant cortices (*D*) compared with WT (*C*). (*E–H*) SEM analysis was performed with E16 cortices. (*G*) In WT mice, radial glial cells are aligned radially in the VZ. (*E*) Their radial fibers make bundles and run perpendicular to the pial surface. (*F*) In GLAST$^{-/-}$/GLT1$^{-/-}$ mutants, the alignment and density of radial glial fibers are destroyed. (*H*) In addition, cells in the VZ lost radial morphology. (*I* and *J*) In contrast, Reelin expression (green) was comparable in WT (*I*) and mutant (*J*) mice at E16. Counterstaining of nuclei was performed with propidium iodide (red). MZ, marginal zone. (Scale bars: *A*, *C*, and *I*, 100 μm; *E* and *G*, 5 μm.)

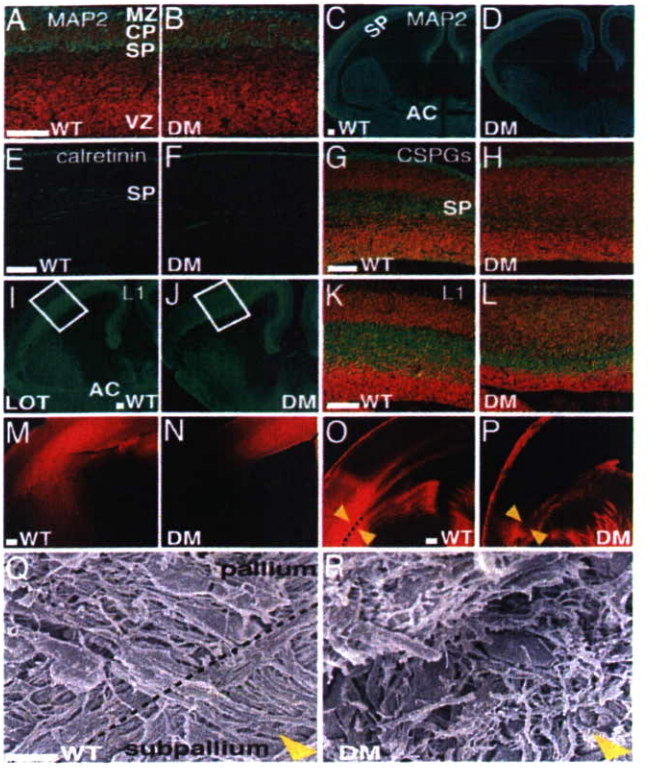

Fig. 5. Loss of SP neurons and impaired cortical connections in GLAST$^{-/-}$/GLT1$^{-/-}$ mutants. (*A–D*) MAP2 staining of E14 (*A* and *B*) and E16 (*C* and *D*) cortices reveals that MAP2-positive SP neurons are difficult to discern in GLAST$^{-/-}$/GLT1$^{-/-}$ mutants (*B* and *D*) at E14 and E16 compared with WT (*A* and *C*). (*E–H*) Immunostaining (green) against calretinin (*E* and *F*) and chondroitin sulfate proteoglycans (CSPGs) (*G* and *H*) on coronal sections of E16 WT (*E* and *G*) and GLAST$^{-/-}$/GLT1$^{-/-}$ mutant (*F* and *H*) cortices shows that SP neurons are mostly missing in mutants. (*I–L*) Immunostaining (green) against L1 on coronal sections of E16 WT (*I* and *K*) and GLAST$^{-/-}$/GLT1$^{-/-}$ mutant (*J* and *L*) cortices reveals defective cortical connections. Boxes in *I* and *J* are enlarged in *K* and *L*, respectively. All nuclei were stained with propidium iodide (red) in *A*, *B*, *G*, *H*, *K*, and *L*. (*M–P*) DiI labeling (red) from cortex (*M* and *N*) and from thalamus (*O* and *P*) at E16 also confirms that TC and CT projections are severely affected in GLAST$^{-/-}$/GLT1$^{-/-}$ mutants. (*M* and *O*) WT. (*N* and *P*) GLAST$^{-/-}$/GLT1$^{-/-}$ mutants. (*Q* and *R*) SEM analysis was performed for the region indicated by arrowheads in *O* and *P* of E16 WT (*Q*) and GLAST$^{-/-}$/GLT1$^{-/-}$ mutant (*R*) brain. In GLAST$^{-/-}$/GLT1$^{-/-}$ mutants, the radial glial fascicle at the pallium–subpallium junction is absent, and TC and CT axons cannot cross the junction. DM, double mutant; MZ, marginal zone; AC, anterior commissure; LOT, lateral olfactory tract. (Scale bars: *A*, *C*, *E*, *G*, *I*, *K*, *M*, and *O*, 100 μm; *Q*, 5 μm.)

Migration of CP Neurons Is Impaired in the GLAST$^{-/-}$/GLT1$^{-/-}$ Cortex. The disturbed laminar organization of the GLAST$^{-/-}$/GLT1$^{-/-}$ mutant cortex suggested that cortical cell migrations were abnormal. To investigate neuronal migration *in vivo*, we injected pregnant mice at E12 or E14 with BrdU and examined the labeling patterns at E16. The mutant E12 neurons were spread in a broader gradient compared with WT (Fig. 3 *I–L*), and the mutant E14 neurons failed to migrate to the CP and remained in the VZ (Fig. 3 *M–P*). Thus, radial migration is impaired in GLAST$^{-/-}$/GLT1$^{-/-}$ mutants. Correct neuronal migration requires both the radial glial fibers, which guide postmitotic neurons during their migration, and Cajal–Retzius neurons, which secrete the Reelin protein and thus have a critical role in radial migration. The alignment and density of radial glial fibers stained with anti-nestin antibody were comparable in WT and mutant E14 cortices (Fig. 4 *A* and *B*), but the disruption of radial fibers was apparent in mutant E16 cortices (Fig. 4 *C* and *D*). SEM analysis also revealed that, at E16, the radial glial fibers in the cerebral wall were disrupted in GLAST$^{-/-}$/GLT1$^{-/-}$ mutants (Fig. 4 *E* and *F*). Furthermore, radial glial cell arrangement was severely disorganized in the VZ of GLAST$^{-/-}$/GLT1$^{-/-}$ mutants (Fig. 4 *G* and *H*). These cells had lost radial morphology but had become round in shape. By contrast, neither the number of Cajal–Retzius neurons nor their immunolabeling intensity for Reelin was changed in the GLAST$^{-/-}$/GLT1$^{-/-}$ cortex (Fig. 4 *I* and *J*). These data suggest that a disrupted radial glial fiber system contributes to the abnormal radial migration of GLAST$^{-/-}$/GLT1$^{-/-}$ mutants.

Lack of SP Neurons and Defective Cortical Connections in the GLAST$^{-/-}$/GLT1$^{-/-}$ Mutants. In the double mutants, the SP is difficult to discern (Fig. 1*F*). Because SP neurons are vulnerable to excitotoxic cell death (23), it is possible that GLAST$^{-/-}$/GLT1$^{-/-}$ mutants may exhibit SP defects. To investigate possible SP defects in double mutants, we studied microtubule-associated protein 2 (MAP2)-positive SP neurons and expression of SP-specific markers, calretinin and chondroitin sulfate proteoglycans (CSPGs). In double mutants, no MAP2-positive SP neurons were detected at E14 or E16 (Fig. 5 *A–D*). Furthermore, calretinin and CSPGs were scarcely present in the SP at E16 (Fig. 5 *E–H*). These results suggest a lack of mature SP neurons in double mutants. SP neurons have been implicated in the development of cortical afferent and efferent connections, including the corticothalamic (CT) and thalamocortical (TC) pathways (23–26). To study these pathways, we used L1 immunostaining and 1,1′-dioctadecyl-3,3,3′,3′-tetramethylindocarbocyanine (DiI) tracing. In WT brains, L1-positive fascicles of CT axons pass through the striatum (Fig. 5*I*). WT L1-positive TC axons leave the diencephalons for the internal capsules and subse-

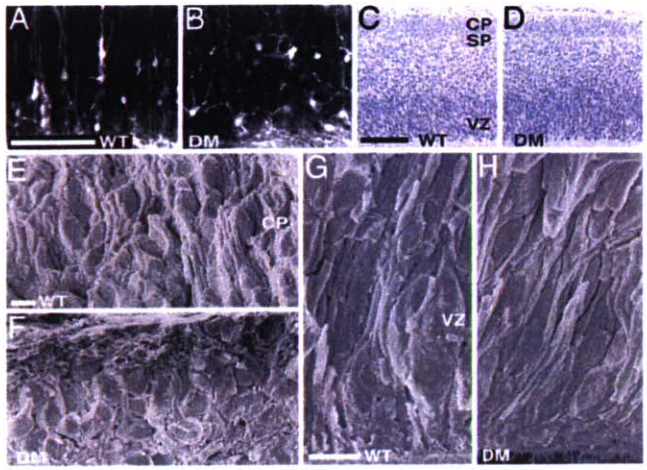

Fig. 6. Impaired maturation of CP neurons in GLAST$^{-/-}$/GLT1$^{-/-}$ mutants. (*A*) At E16, pyramidal-like retrogradely labeled cells are observed in the CP of WT mice after DiI injection in the thalamus. (*B*) In mutants, the morphology and neurite extension of the retrogradely labeled cells were affected. (*C* and *D*) Coronal sections of neocortex at E14 from WT mice (*C*) and GLAST$^{-/-}$/GLT1$^{-/-}$ mutants (*D*) stained with hematoxylin. (*E–H*) SEM analysis was performed with E14 cortices. Although the hematoxylin staining could not reveal impaired maturation of CP neurons in mutants at E14, SEM analysis revealed that the cellular morphology was affected in GLAST$^{-/-}$/GLT1$^{-/-}$ mutants (*F*) compared with WT (*E*). In contrast, the cellular morphology in the VZ was comparable in WT (*G*) and mutant (*H*) E14 cortices. DM, double mutants. (Scale bars: *A* and *C*, 100 μm; *E* and *G*, 5 μm.)

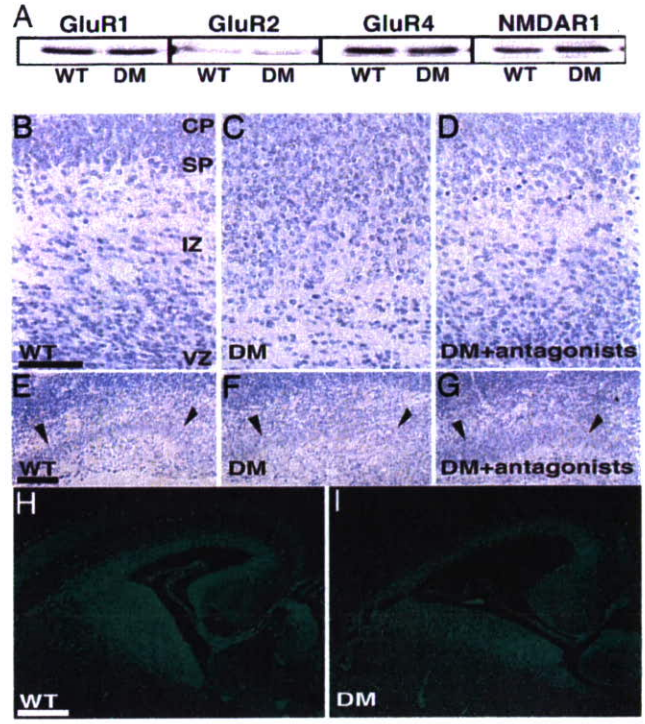

Fig. 7. Partial rescue of the GLAST$^{-/-}$/GLT1$^{-/-}$ mutant brain phenotype by injection of glutamate receptor antagonists. (*A*) The relative expression of the glutamate receptors GluR1, GluR2, and GluR4 and NMDA receptor 1 was unchanged in GLAST$^{-/-}$/GLT1$^{-/-}$ mice compared with WT animals. (*B–G*) Coronal sections of cortex (*B–D*) and sagittal sections of hippocampus (*E–G*) of E16 WT (*B* and *E*), GLAST$^{-/-}$/GLT1$^{-/-}$ (*C* and *F*), and GLAST$^{-/-}$/GLT1$^{-/-}$ mice treated from E8 to E16 with 2,3-dihydroxy-6-nitro-7-sulfamoylbenzo[*f*]quinoxaline (NBQX) and CGS-19755 (*D* and *G*) stained with hematoxylin. Injections of both NBQX and CGS-19755 resulted in a partial rescue of the abnormal stratification of the mutant cerebral cortex and hippocampus. Arrowheads in *E–G* indicate the pyramidal cell layer in the hippocampus. (*H* and *I*) *In situ* hybridization using NARG1 riboprobe on coronal sections of E16 WT (*H*) and GLAST$^{-/-}$/GLT1$^{-/-}$ mutants (*I*). The expression of NARG1 was down-regulated in mutants. DM, double mutants; IZ, intermediate zone. (Scale bar: 100 μm.)

quently enter the cortex at E16 (Fig. 5 *I* and *K*). In double mutants, L1-poisitive TC axons scarcely innervated the cortex (Fig. 5 *J* and *L*). DiI injection in the cortex at E16 revealed that CT axons did not exit the telencephalon in GLAST$^{-/-}$/GLT1$^{-/-}$ mutants (Fig. 5 *M* and *N*). DiI injection in the thalamus at E16 confirmed that TC axons did not enter the GLAST$^{-/-}$/GLT1$^{-/-}$ cortex (Fig. 5 *O* and *P*). SEM analysis of GLAST$^{-/-}$/GLT1$^{-/-}$ double mutants revealed that, at E16, the radial glial fascicle at the pallial–subpallial boundary was absent and that CT and TC axons could not cross the pallial–subpallial boundary (Fig. 5 *Q* and *R*). The corpus callosum did not cross the midline but formed a Probst bundle (Fig. 1*B*). Also, the anterior commissure was absent in mutants (Fig. 1*D*). These results indicate that the TC, CT, and callosal projections are severely affected in GLAST$^{-/-}$/GLT1$^{-/-}$ mutants.

Maturation of CP Neurons Is Impaired in the GLAST$^{-/-}$/GLT1$^{-/-}$ Mutants. At E16, pyramidal-like retrogradely labeled cells in the CP after a DiI injection in thalamus were observed in WT mice (Fig. 6*A*). In contrast, the morphology and neurite outgrowth of the retrogradely labeled cells in the CP were affected in mutant mice (Fig. 6*B*). To determine the onset of these changes, we examined E14 GLAST$^{-/-}$/GLT1$^{-/-}$ mutant cortex. Although hematoxylin staining did not show abnormal morphology of CP neurons in the GLAST$^{-/-}$/GLT1$^{-/-}$ mutants at E14 (Fig. 6 *C* and *D*), SEM analysis of GLAST$^{-/-}$/GLT1$^{-/-}$ mutants showed that, at E14, the radial distribution of the CP neurons and their neurites was not conspicuous; these cells had lost their pyramidal-like morphology and had become round in shape (Fig. 6 *E* and *F*). In contrast, the alignment and density of radial glial cells in the VZ were comparable in WT and mutant E14 cortices (Fig. 6 *G* and *H*). These results indicate that maturation of CP neurons is impaired in the GLAST$^{-/-}$/GLT1$^{-/-}$ mutants from E14 onward, whereas abnormal maturation of radial glial cells in the VZ was apparent at E16 (Fig. 4 *G* and *H*).

Partial Rescue of the GLAST$^{-/-}$/GLT1$^{-/-}$ Brain Phenotypes by Glutamate Receptor Antagonists. Because we previously showed that basal levels of extracellular glutamate in the hippocampus of GLT1 mutant mice were significantly higher than those of WT mice (27), it is reasonable to expect that genetic deletion of both GLT1 and GLAST would bring about an increase in extracellular glutamate levels, resulting in cortical malformation by excess activation of glutamate receptors. To assess this hypothesis, we first examined whether expression of glutamate receptors is affected in the GLAST$^{-/-}$/GLT1$^{-/-}$ mutant cortex. The relative expression of the glutamate receptors GluR1, GluR2, and GluR4 and NMDA receptor 1 was unchanged in GLAST$^{-/-}$/GLT1$^{-/-}$ mice compared with WT animals (n = 3 for each) (Fig. 7*A*). Next, we examined whether the GLAST$^{-/-}$/GLT1$^{-/-}$ brain phenotype could be reversed by pharmacological administration of glutamate receptor antagonists. Injections of both the α-amino-3-hydroxy-5-methyl-4-isoxazolepropionic acid (AMPA) receptor antagonist 2,3-dihydroxy-6-nitro-7-sulfamoylbenzo[*f*]quinoxaline (NBQX) and the NMDA receptor antagonist CGS-19755 in pregnant mice between E8 and E16 resulted in a partial rescue of the abnormal stratification of the mutant cerebral cortex (Fig. 7 *B–D*) and hippocampus (Fig. 7 *E* and *G*). In GLAST$^{-/-}$/GLT1$^{-/-}$ mutants treated with glutamate receptor antagonists, the cerebral cortex showed some restoration of laminar structure, although it remained

less organized than in WT mice (Fig. 7 *B–D*). The hippocampus of GLAST$^{-/-}$/GLT1$^{-/-}$ mice is characterized by loose packing of pyramidal neurons (Fig. 7*F*). In contrast, GLAST$^{-/-}$/GLT1$^{-/-}$ mice treated with glutamate receptor antagonists had hippocampal formations that seemed almost indistinguishable from WT hippocampus (Fig. 7 *E* and *G*). The excess activation of the NMDA receptors in GLAST$^{-/-}$/GLT1$^{-/-}$ mutant brains was also suggested by the examination of expression levels of NMDA receptor-regulated gene 1 (NARG1). A previous study demonstrated that NARG1 is down-regulated by NMDA receptor activation (28). We found that NARG1 mRNA expression was down-regulated in GLAST$^{-/-}$/GLT1$^{-/-}$ mutant brains by *in situ* hybridization (Fig. 7 *H* and *I*) and real-time quantitative PCR (Fig. 11, which is published as supporting information on the PNAS web site). Injection of the NMDA receptor antagonist CGS-19755 alone could not rescue the GLAST$^{-/-}$/GLT1$^{-/-}$ brain phenotypes. Moreover, both the AMPA receptor antagonist and the NMDA receptor antagonist only partially rescued the cortical malformation of mutant mice, suggesting that, in addition to excess activation of both AMPA and NMDA receptors, overactivation of other glutamate receptors, including metabotropic glutamate receptors, may contribute to the multiple severe defects in GLAST$^{-/-}$/GLT1$^{-/-}$ mutants.

Oxidative Glutamate Toxicity Does Not Contribute to the Cortical Malformation of GLAST$^{-/-}$/GLT1$^{-/-}$ Mice. Excessive extracellular glutamate leads to cell injury by means of both glutamate receptor-mediated and glutamate receptor-independent mechanisms (29). Glutamate receptor-independent toxicity is caused by oxidative glutamate toxicity. In oxidative glutamate toxicity, high levels of glutamate block the cystine/glutamate exchange system Xc^-, resulting in glutathione depletion and cell injury (30). To determine whether oxidative glutamate toxicity is involved in the cortical malformation of GLAST$^{-/-}$/GLT1$^{-/-}$ mice, we measured the total cortical glutathione levels. Total glutathione levels were slightly increased in the cortex of GLAST$^{-/-}$/GLT1$^{-/-}$ mice at E16 compared with WT levels (Fig. 12, which is published as supporting information on the PNAS web site), demonstrating that oxidative glutamate toxicity does not play a significant role in the cortical malformation of GLAST$^{-/-}$/GLT1$^{-/-}$ mice.

Discussion

A large body of *in vitro* evidence indicates that the neurotransmitter glutamate acts to influence earlier developmental events, such as proliferation, migration, and differentiation (4–7). However, nearly all of the genetic experiments to date, in which glutamatergic signaling was blocked, have shown little, if any, developmental defects (8–14). Our work represents a unique analysis of the direct consequences on brain development of extracellular glutamate buildup due to the depletion of glutamate transporters. In contrast to loss-of-function studies, *in vivo* excess activation of glutamate receptors can modulate brain maturation, such as stem cell proliferation, radial migration, survival of SP neurons, and neuronal differentiation, including neurite elongation and path finding. This discrepancy may be due to compensation by other neurotransmitters such as GABA, acetylcholine (Ach), and glycine, all of which can depolarize embryonic cortical neurons as does glutamate (31). GABA is also one of the most abundant neurotransmitters detected during mammalian brain development, and its involvement in shaping brain development has also been suggested by recent *in vitro* investigations (5, 32, 33). However, mice lacking the two primary GABA biosynthetic enzymes, GAD65 and GAD67, show no discernible defects of neural development despite having only 0.02% of the normal GABA content (34). This discrepancy might also be due to compensation by other neurotransmitters *in vivo*. Glutamate, GABA, Ach, and glycine can all depolarize embryonic cortical neurons, so pathways involving more than one of these transmitters could potentially show mitigated severity of defects in single-neurotransmitter loss-of-function mutations. In the future, it will be important to analyze the direct consequences of overactivation of individual neurotransmitter receptors. Such studies could reveal functional roles of early appearing transmitter signaling during development.

The prevailing view of CNS development is that neural activity is, for the most part, important only in the refinement of axonal projections and synaptic connections, whereas early development of the nervous system is likely to be genetically programmed. Two recent studies have challenged this view by providing evidence that neural activity is required for spinal motor neurons to make accurate early path-finding decisions (35) and for embryonic spinal cord neurons to determine which types of neurotransmitters to produce (36). Combined with these studies, the present study suggests that neural activity is likely to be important in shaping early brain development and that glutamate, as a key mediator of neural activity, may play an important role in shaping the early CNS development. For these influences to be physiologically relevant, however, glutamate must be released at an early developmental stage and diffuse to stimulate glutamate receptors. Several observations support this hypothesis: (*i*) functional glutamate receptors are expressed by neuronal precursors and neurons of several brain areas at a very early stage (3, 37), (*ii*) exocytosis of glutamate occurs from growing axons and cones before synapse formation (38), (*iii*) paracrine nonvesicular release of glutamate exists before synapse formation and modulates neuronal migration (39, 40), and (*iv*) an efficient glutamate transport system is operative at early developmental stages (39). Depending on the neural activity and the location and properties of glutamate receptors and transporters, it is possible that excess activation of glutamate receptors can occur and modulate brain development. Therefore, normal brain development requires tight control of extracellular glutamate by the glutamate transporters GLAST and GLT1. This hypothesis was also confirmed by the severe developmental defects that were observed in the regions of the brain where both GLAST and GLT1 are expressed, such as the inner half of the cortex, the pallium–subpallium boundary, and the SP neurons (Fig. 13, which is published as supporting information on the PNAS web site). GLAST$^{-/-}$/GLT1$^{-/-}$ double mutants have enabled us to clarify how glutamatergic signaling regulates the molecular pathways that control brain development.

Previous *in vitro* studies demonstrated that glutamate is involved in modulating the radial migration of cortical projection neurons. Blockade of NMDA receptors decreases cell migration, whereas enhancement of NMDA receptor activity or inhibition of extracellular glutamate uptake increases the rate of cell movement (4, 7). Interestingly, radial migration is impaired in GLAST$^{-/-}$/GLT1$^{-/-}$ double mutants, in which excess activation of the NMDA receptor may occur. This impairment could be attributed to the fact that excess activation of glutamate receptors in GLAST$^{-/-}$/GLT1$^{-/-}$ double mutants leads to disruption of the radial glial fiber system. Recent studies have indicated that glutamate released from corticofugal axons could lead to NMDA and AMPA/kainate receptor activation in tangentially migrating cells and thereby modulate their response to guidance cues (41, 42). Furthermore, GLT1 is expressed in corticofugal axons. Future experiments investigating the tangential migration of interneurons in GLAST$^{-/-}$/GLT1$^{-/-}$ double mutants may clarify the functional significance of glutamate for tangential migration as well as radial migration.

It has been shown that SP cells are necessary for the development of many efferent and afferent cortical connections (23–26). We found that SP neurons were deficient in the neocortex of GLAST$^{-/-}$/GLT1$^{-/-}$ mutants from E14 onward. Consistent with the defect in SP neurons, TC and CT projections were lacking in mutant mice.

Abnormal development of the brain during fetal life is now thought to contribute to the etiology of many neurological disorders that manifest throughout life (43). Cerebral hypoxia-ischemia is considered to be a major cause of perinatal brain injury. A dysfunction of glutamate transporters and the resulting excess glutamate are important pathophysiological mechanisms in brain injury after hypoxia-ischemia. Therefore, GLAST$^{-/-}$/GLT1$^{-/-}$ mutants may be useful for characterizing lesions formed in response to hypoxia-ischemia and for developing neuroprotective strategies to reduce the burden of altered brain growth and poor functional and behavioral outcomes (44).

Materials and Methods

Mice. The GLT1, GLAST, and EAAC1 mutant mice are described in refs. 17–19. To generate all combinations of double mutants, double-heterozygous mice (GLT1$^{+/-}$/GLAST$^{+/-}$, GLAST$^{+/-}$/EAAC1$^{+/-}$, and EAAC1$^{+/-}$/GLT1$^{+/-}$) were crossed. All mice were on a C57BL/6J background. The day of vaginal plug detection was designated as E0.5.

Histological Analysis, BrdU Labeling, TUNEL Assay, Western Blot Analysis, Real-Time PCR, and Glutathione Assay. All detailed information specific to the experiments described here can be found in *Supporting Materials and Methods*, which is published as supporting information on the PNAS web site.

Effect of AMPA and NMDA Receptor Antagonism on Brain Abnormalities of Mutant Mice. This experiment was performed as described in ref. 45. Between E8 and E16, pregnant mice received i.p. injections of the AMPA and NMDA receptor antagonists. Detailed procedures are described in *Supporting Materials and Methods*.

We thank R. A. Corriveau (Wayne State University, Detroit, MI) for his gift of the NARG1 probe and H. Kamiguchi (RIKEN Brain Science Institute) for his gift of the L1 antibody. This work was supported by research grants from RIKEN Brain Science Institute; a grant-in-aid for Scientific Research from the Japan Society for the Promotion of Sciences; and a grant-in-aid for Scientific Research on Priority Areas from the Ministry of Education, Culture, Sports, and Technology of Japan (to K. Tanaka).

1. Cohen-Cory, S. (2002) *Science* **298,** 770–776.
2. Ben-Ari, Y. (2001) *Trends Neurosci.* **24,** 353–360.
3. Nguyen, L., Rigo, J. M., Rocher, V., Belachew, S., Malgrange, B., Rogister, B., Leprince, P. & Moonen, G. (2001) *Cell Tissue Res.* **305,** 187–202.
4. Komuro, H. & Rakic, P. (1993) *Science* **260,** 95–97.
5. LoTurco, J. J., Owens, D. F., Heath, M. J., Davis, M. B. & Kriegstein, A. R. (1995) *Neuron* **15,** 1287–1298.
6. Ikonomidou, C., Bosch, F., Miksa, M., Bittigau, P., Vockler, J., Dikranian, K., Tenkova, T. I., Stefovska, V., Turski, L. & Olney, J. W. (1999) *Science* **283,** 70–74.
7. Behar, T. N., Scott, C. A., Greene, C. L., Wen, X., Smith, S. V., Maric, D., Liu, Q. Y., Colton, C. A. & Barker, J. L. (1999) *J. Neurosci.* **19,** 4449–4461.
8. Kutsuwada, T., Sakimura, K., Manabe, T., Takayama, C., Katakura, N., Kushiya, E., Natsume, R., Watanabe, M., Inoue, Y., Yagi, T., *et al.* (1996) *Neuron* **16,** 333–344.
9. Messersmith, E. K., Feller, M. B., Zhang, H. & Shatz, C. J. (1997) *Mol. Cell. Neurosci.* **9,** 347–357.
10. Zamanillo, D., Sprengel, R., Hvalby, O., Jensen, V., Burnashev, N., Rozov, A., Kaiser, K. M., Koster, H. J., Borchardt, T., Worley, P., *et al.* (1999) *Science* **284,** 1805–1811.
11. Meng, Y., Zhang, Y. & Jia, Z. (2003) *Neuron* **39,** 163–176.
12. Verhage, M., Maia, A. S., Plomp, J. J., Brussaard, A. B., Heeroma, J. H., Vermeer, H., Toonen, R. F., Hammer, R. E., van den Berg, T. K., Missler, M., *et al.* (2000) *Science* **287,** 864–869.
13. Wojcik, S. M., Rhee, J. S., Herzog, E., Sigler, A., Jahn, R., Takamori, S., Brose N. & Rosenmund, C. (2004) *Proc. Natl. Acad. Sci. USA.* **101,** 7158–7163.
14. Fremeau, R. T., Jr., Kam, K., Qureshi, T., Johnson, J., Copenhagen, D. R., Storm-Mathisen, J., Chaudhry, F. A., Nicoll, R. A. & Edwards, R. H. (2004) *Science* **304,** 1815–1819.
15. Tanaka, K. (2000) *Neurosci. Res.* **37,** 15–19.
16. Shibata, T., Watanabe, M., Tanaka, K., Wada, K. & Inoue, Y. (1996) *NeuroReport* **7,** 705–709.
17. Tanaka, K., Watase, K., Manabe, T., Yamada, K., Watanabe, M., Takahashi, K., Iwama, H., Nishikawa, T., Ichihara, N., Kikuchi, T., *et al.* (1997) *Science* **276,** 1699–1702.
18. Peghini, P., Janzen, J. & Stoffel, W. (1997) *EMBO J.* **16,** 3822–3832.
19. Watase, K., Hashimoto, K., Kano, M., Yamada, K., Watanabe, M., Inoue, Y., Okuyama, S., Sakagawa, T., Ogawa, S., Kawashima, N., *et al.* (1998) *Eur. J. Neurosci.* **10,** 976–988.
20. Danbolt, N. C. (2001) *Prog. Neurobiol.* **65,** 1–105.
21. Chen, W., Mahadomrongkul, V., Berger, U. A., Bassan, M., DeSilva, T., Tanaka, K., Irwin, N., Aoki, C. & Rosenberg, P. A. (2004) *J. Neurosci.* **24,** 1136–1148.
22. Yamada, K., Watanabe, M., Shibata, T., Nagashima, M., Tanaka, K. & Inoue, Y. (1998) *J. Neurosci.* **18,** 5706–5713.
23. McConnell, S. K., Ghosh, A. & Shatz, C. J. (1994) *Neuroscience* **14,** 1892–1907.
24. Hevner, R. F., Shi, L., Justice, N., Hsueh, Y., Sheng, M., Smiga, S., Bulfone, A., Goffinet, A. M., Campagnoni, A. T. & Rubenstein, J. L. (2001) *Neuron* **29,** 353–366.
25. Ghosh, A., Antonini, A., McConnell, S. K. & Shatz, C. J. (1990) *Nature* **347,** 179–181.
26. De Carlos, J. A. & O'Leary, D. D. (1992) *J. Neurosci.* **12,** 1194–1211.
27. Mitani, A. & Tanaka, K. (2003) *J. Neurosci.* **23,** 7176–7182.
28. Sugiura, N., Patel, R. G. & Corriveau, R. A. (2001) *J. Biol. Chem.* **276,** 14257–14263.
29. Schubert, D. & Piasecki, D. (2001) *J. Neurosci.* **21,** 7455–7462.
30. Rimaniol, A. C., Mialocq, P., Clayette, P., Dormont, D. & Gras, G. (2001) *Am. J. Physiol.* **281,** C1964–C1970.
31. Ben-Ari, Y. (2002) *Nat. Rev. Neurosci.* **3,** 728–739.
32. Behar, T. N., Li, Y. X., Tran, H. T., Ma, W., Dunlap, V., Scott, C. & Barker, J. L. (1996) *J. Neurosci.* **16,** 1808–1818.
33. Obata, K. (1997) *Dev. Neurosci.* **19,** 117–119.
34. Ji, F., Kanbara, N. & Obata, K. (1999) *Neurosci. Res.* **33,** 187–194.
35. Hanson, M. G. & Landmesser, L. T. (2004) *Neuron* **43,** 687–701.
36. Borodinsky, L. N., Root, C. M., Cronin, J. A., Sann S. B., Gu, X. & Spitzer, N. C. (2004) *Nature* **429,** 523–530.
37. Lujan, R., Shigemoto, R. & Lopez-Bendito, G. (2005) *Neuroscience* **130,** 567–580.
38. Socda, H., Tatsumi, H. & Katayama, Y. (1997) *Neuroscience* **77,** 1187–1189.
39. Demarque, M., Represa, A., Becq, H., Khalilov, I., Ben-Ari, Y. & Anirksztejn, L. (2002) *Neuron* **36,** 1051–1061.
40. Manent, J. B., Demarque, M., Jorquera, I., Pellegrino, C., Ben-Ari, Y., Aniksztejn, L. & Represa, A. (2005) *J. Neurosci.* **25,** 4755–4765.
41. Poluch, S., Drian, M. J., Durand, M., Astier, C., Benyamin, Y. & Konig, N. (2001) *J. Neurosci. Res.* **63,** 35–44.
42. Soria, J. M. & Valdeolmillos, M. (2002) *Cereb. Cortex* **12,** 831–839.
43. Rees, S. & Inder, T. (2005) *Early Hum. Dev.* **81,** 753–761.
44. Tanaka, K. (2005) *Trends Mol. Med.* **11,** 259–262.
45. Simonian, S. X. & Herbison, A. E. (2001) *J. Neurosci.* **21,** 934–943.

0888-8809/08/$15.00/0
Printed in U.S.A.

Molecular Endocrinology 22(1):56–64

doi: 10.1210/me.2007-0290

Nuclear Receptor TLX Regulates Cell Cycle Progression in Neural Stem Cells of the Developing Brain

Wenwu Li, Guoqiang Sun, Su Yang, Qiuhao Qu, Kinichi Nakashima, and Yanhong Shi

Neuroscience Division (W.L., G.S., S.Y., Q.Q., Y.S.), Beckman Research Institute of City of Hope, Duarte, California 91010; and Laboratory of Molecular Neuroscience (K.N.), Graduate School of Biological Sciences, Nara Institute of Science and Technology, Ikoma 630-0101, Japan

TLX is an orphan nuclear receptor that is expressed exclusively in vertebrate forebrains. Although TLX is known to be expressed in embryonic brains, the mechanism by which it influences neural development remains largely unknown. We show here that TLX is expressed specifically in periventricular neural stem cells in embryonic brains. Significant thinning of neocortex was observed in embryonic d 14.5 TLX-null brains with reduced nestin labeling and decreased cell proliferation in the germinal zone. Cell cycle analysis revealed both prolonged cell cycles and increased cell cycle exit in TLX-null embryonic brains. Increased expression of a cyclin-dependent kinase inhibitor p21 and decreased expression of cyclin D1 provide a molecular basis for the deficiency of cell cycle progression in embryonic brains of TLX-null mice. Furthermore, transient knockdown of TLX by *in utero* electroporation led to precocious cell cycle exit and differentiation of neural stem cells followed by outward migration. Together these results indicate that TLX plays an important role in neural development by regulating cell cycle progression and exit of neural stem cells in the developing brain. (*Molecular Endocrinology* 22: 56–64, 2008)

NUCLEAR RECEPTORS ARE ligand-dependent transcription factors that have important roles in several biological processes, including cell proliferation, differentiation, and cellular homeostasis (1). TLX was initially identified as an orphan nuclear receptor that is homologous to the *Drosophila* tailless gene and plays an important role in vertebrate brain functions (2). Expression of TLX in the mouse starts at embryonic d 8 (E8), peaks at E13.5, and decreases by E16, with barely detectable levels at birth. TLX expression increases again after birth with high levels of expression in adult brains (3). The biphasic expression pattern of TLX suggests that TLX could play a role in both brain development and adult brain function.

We have shown that TLX is an essential regulator of neural stem cell maintenance and self-renewal in the adult brain (4). The TLX-expressing cells isolated from adult TLX-heterozygote brains can proliferate, self-renew, and differentiate into all three major neural cell types *in vitro*. By contrast, TLX-null cells isolated from the brains of adult TLX-mutant mice fail to proliferate. Reintroducing TLX into TLX-null cells rescued their ability to proliferate and self-renew (4).

Mature TLX knockout mice suffer from severe limbic defects, aggressiveness, decreased copulation, progressively violent behavior, and retinopathies (4–12). Fierce mice, a natural mutant homozygous for a deletion of TLX, show pathological aggression (13), similar to the TLX knockout mice. Introducing the human TLX gene into fierce mice ameliorates the brain and eye abnormalities (14), suggesting that the mechanisms underlying the behavioral abnormalities may be conserved in humans. Therefore, mutation of the TLX gene may contribute to human behavioral disorders.

Although the role of TLX in adult neural stem cells is unfolding, the mechanism by which it influences neural development remains unknown. In this study, we show that TLX is specifically expressed in the periventricular neural stem cells in the developing brain. Using TLX knockout mice we show that loss of TLX expression led to significant thinning of embryonic neocortex, reduced nestin labeling, and decreased cell proliferation in the ventricular zone (VZ) of E14.5 brains. Both prolonged cell cycles and reduced cell cycle reentry were observed in the VZ of TLX−/− embryonic brains. Moreover, TLX short interfering RNA (siRNA) treatment through *in utero* electroporation triggered cell cycle exit and neuronal differentiation of neural stem cells and outward migration of the differentiated cells in the embryonic neocortex. These results suggest that TLX is an important regulator of embryonic neural stem cell proliferation and differentiation through cell cycle control.

First Published Online September 27, 2007

Abbreviations: BrdU, Bromodeoxyuridine; DCX, doublecortin; E8, embryonic d 8; β-gal, β-galactosidase; GFP, green fluorescent protein; NeuN, neuronal nuclei; PPARγ, peroxisomal proliferator-activated receptor-γ; siRNA, short interfering RNA; TUNEL, terminal transferase dUTP nick end labeling; VZ, ventricular zone; X-gal, 5-bromo-4-chloro-3-indolyl-β-galactopyranoside.

***Molecular Endocrinology* is published monthly by The Endocrine Society (http://www.endo-society.org), the foremost professional society serving the endocrine community.**